Taylor & Francis
Taylor & Francis Group

RESEARCH PAPER

🔓 OPEN ACCESS   Check for updates

AMPK protects against alcohol-induced liver injury through UQCRC2 to up-regulate mitophagy

Xinyi Lu [a,#], Wenting Xuan[b,#], Juanjuan Li[a], Hongwei Yao[a], Cheng Huang[a], and Jun Li[a]

[a]Inflammation and Immune Mediated Diseases Laboratory of Anhui Province, School of Pharmacy, Anhui Medical University, Hefei, Anhui, China; [b]Department of Anesthesiology, Drum Tower Hospital, Medical College of Nanjing University, Nanjing, China

ABSTRACT

Recent reports indicated that mitophagy protects against alcohol-induced liver injury, which helps remove damaged mitochondria to reduce the accumulation of reactive oxygen species (ROS). AMP-activated protein kinase (AMPK) has been recently used in ALD (alcoholic liver disease) and mitochondrial dysfunction research. However, the inner mechanism, whether AMPK can regulate mitophagy in ALD, remains unknown. Here we found that AMPK can significantly reduce alcohol-induced liver injury and enhances hepatocytes' mitophagy level. Next, we identified that AMPK rescued alcohol-induced low expression of UQCRC2 (ubiquinol-cytochrome c reductase core protein 2). Interestingly, UQCRC2 knockdown (KD) treatment causes impaired mitophagy, whereas UQCRC2 overexpression (OE) can significantly increase mitophagy to attenuate liver injury. Also, we identified that AMPK indirectly upregulates UQCRC2 protein level, and RNA-seq, chromatin immunoprecipation (ChIP) assay, bioinformatics, and luciferase assays helped us understand that AMPK enhanced *UQCRC2* gene transcription through activating NFE2L2/NRF2 (nuclear factor, erythroid 2 like 2). Our results demonstrate that AMPK regulating UQCRC2 is a significant mitochondrial event in mitophagy. It identifies a new signaling axis, AMPK-NFE2L2-UQCRC2, in the regulation of mitophagy levels in the liver, suggesting a possible therapeutic strategy to treat ALD.

Abbreviations: AAV: AENO-associated virus; ALD: alcoholic liver disease; AMPK: AMP-activated protein kinase; BUN: blood urea nitrogen; H&E: hematoxylin and eosin; CCCP: carbonyl cyanide 3-chlorophenyl-hydrazone; ChIP: chromatin immunoprecipitation assay; CO-IP: co-immunoprecipitation; COPD: chronic obstructive pulmonary disease; EM: electron microscope; GOT1/AST: glutamic-oxaloacetic transaminase 1; GPT/ALT: glutamic—pyruvic transaminase; IF: immunofluorescence; IHC: immunohistochemistry; KD: knockdown; MAP1LC3/LC3: microtubule associated protein 1 light chain protein 3; MTDR: MitoTracker Deep Red; NFE2L2/NRF2: nuclear factor, erythroid 2 like 2; mtDNA: mitochondrial DNA; MTRC: MitoTracker Red CMXRos; OCR: Oxygen consumption rate; OE: overexpress; PINK1: PTEN induced kinase 1; qRT-PCR: quantitative real-time PCR; ROS: reactive oxygen species; SD: standard deviation; SOD2: superoxide dismutase 2; UQCRC2: ubiquinol-cytochrome c reductase core protein 2; WB: western blot; ΔΨ: mitochondrial membrane potential;

Introduction

ALD is a common health problem [1]. ALD pathogenesis begins with liver steatosis, reversible pathogenesis caused by alcohol consumption. Continuous alcohol abuse may cause steatohepatitis, fibrosis, cirrhosis, and even hepatocellular carcinoma. The mechanisms of the progression of ALD pathogenesis are still not completely understood [2,3]. Thus, further investigations into the mechanisms involved in ALD pathogenesis are needed for the development of next-generation therapeutics that attenuates alcohol-induced liver disease.

Autophagy is a protective process that initiates the lysosomal degradation of cellular components. This process removes damaged organelles and protein aggregates to prevent cell death and tissue injury [4]. Selective autophagy plays a critical role in ALD. Mitophagy, which selectively removes damaged mitochondria, may be a protective mechanism for ALD, and it can attenuate cellular reactive oxygen species (ROS) accumulation, mitochondrial DNA (mtDNA) damage, and accumulation of aged or damaged mitochondrial [5,6]. A report also indicated that MIEF1, a mitophagy related protein deficiency, sensitized cytosolic BAX to translocate onto the mitochondria, which caused cell death [7]. In addition, our previous study indicated that defective mitophagy induces cellular senescence and inflammatory responses in cigarette smoke-induced chronic obstructive pulmonary disease (COPD) [8]. Consequently, the mechanisms of mitophagy and mitochondrial dysfunction in ALD still need to be investigated.

The primordial role of AMPK as an energy sensor has been co-opted in higher eukaryotes to coordinate growth and metabolism in specialized tissues at the whole-body level [9]. Previous articles indicated that AMPK significantly attenuates symptoms of nonalcoholic fatty liver disease (NAFLD) due to its decent protective effects in decreasing hepatic gluconeogenesis and enhancing glucose uptake in muscle [10,11]. The function of AMPK in mitophagy was also highlighted recently. For example, a study convincingly demonstrated that AMPK activation protects against MLL-AF9 induced metabolic stress in a mouse model of leukemia, because AMPK signaling responds to energy stress by the direct activation of FIS1 (fission, mitochondrial 1), and regulation of mitophagy activity under mitochondria stress [12]. Consequently, AMPK deserves our attention in ALD research due to its diverse function in cell pathways network. In this study, we observed that AMPK indirectly upregulated UQCRC2 expression to enhance mitophagy, which reveals a strategy for targeting mitophagy to attenuate ALD progression.

Results

AMPK attenuates alcohol-induced liver injury and mitochondrial injury

To investigate the function of AMPK in ALD, we treated mice with metformin. Metformin is a classical AMPK agonist, which can significantly increase the p-AMPK level. At first, we used GPT/ALT, GOT1/AST, BUN methods to identify the toxicity of metformin in the liver and kidney. Interestingly, we found that 50, 150, 250 mg/kg concentration of metformin cannot cause liver or kidney toxicity (Figure S1A-C). Ethanol significantly upregulated GPT and GOT1 levels, whereas 150 mg/kg metformin considerably attenuated ethanol-induced liver injury (Figure S1DE). The BUN experiments show that alcohol could not cause kidney injury, and metformin could not cause kidney toxicity in ethanol-treated mice (Figure S1F). Interestingly, the western blot results show that ethanol slightly enhanced the p-AMPK level (1.8-fold vs control), whereas metformin (150 mg/kg) significantly improved the p-AMPK level (more than 8-fold vs control) (Figure S1G). Furthermore, hematoxylin and eosin (H&E) (Figure S1H) and oil red staining results (Figure S1I) show that alcohol caused vesicular degeneration and lipid accumulation in the liver, whereas metformin (150 mg/kg) can attenuate those symptoms. Next, we identified the ethanol and metformin concentration in AML-12 cell experiments. The CCK-8 tests show that 200 mM ethanol might cause cell injury (Figure S1J), and we selected this ethanol concentration. A previous article indicated that 3.4–6.4 mM metformin activated LC3 in vitro [13]. Our results show that 3.2 mM metformin could not cause cell injury (Figure S1K), and 3.2 mM metformin significantly upregulated the p-AMPK level (Figure S1L).

In this study, we further built a kind of long-term binge ALD mice model (at most 2 months). According to HE staining results, we found that more lipid accumulation might develop in mice liver with long time ethanol-fed

(Figure S1M). Interestingly, the WB results show that p-AMPK may express a high level in the initial stage (2.0-fold vs control), whereas only 0.3 fold were seen in 2-months-fed mice liver (Figure S1N).

Then, we investigated the AMPK functions on mitochondria. According to electron microscopy (EM) pictures, liver samples from ethanol-fed mice showed decreased mitochondria number, as well as destroyed mitochondrial structure (edema mitochondrial). In contrast, metformin treatment increased the mitochondrial numbers and protect mitochondrial structure (Figure 1AB). Next, we detected the mtDNA level in mice serum to identify the mitochondria injury level. mtDNA only can be detected when many hepatocytes necrosis or apoptosis with the mitochondria injury. qRT-PCR results showed that ethanol destroyed mitochondria, and metformin significantly attenuated alcohol-induced mitochondria injury (Figure 1 C). We also stained AML-12 cells with MitoTracker Red CMXRos (MTRC) to detect the mtROS level, and results showed that ethanol caused a high mtROS level compared with control, whereas metformin reduced mtROS accumulation (Figure 1 DE). These experiments suggest that AMPK may attenuate alcohol-induced mitochondria injury. Furthermore, the western blot results show that ethanol-induced slight autophagy-flux (LC3-II:LC3-I, SQSTM1/p62), and AMPK can significantly enhance total autophagy level in mice and AML-12 cells (Figure 1 FG).

AMPK upregulates mitophagy level

Furthermore, we wanted to identify whether AMPK protects mitochondria via mitophagy. Firstly, we used plasmid to transfect mito timer in AML-12 cells, and we found that ethanol slightly increased the 500:583 nm (green:red) ratio, and metformin (AMPK agonist) significantly increased its fluorescence shifts from green to red (Figure 2 A). As expected, ethanol increased the MitoTracker Deep Red (MTDR) level, and metformin significantly enhances its fluorescence signal (Figure 2 B). The mtKeima experiments also show that ethanol increased mitophagy level in AML-12 cells, and metformin could significantly increase mitophagy level (Figure 2 C). The IF pictures show that mitochondria translocation of LC3 had a slight increase in ethanol treatment mice, and metformin significantly increased the mitochondria translocation level (Figure 2 DE). Next, we detected PRKN and PINK1 proteins level. According to WB (whole cell lysates results), we found that alcohol enhanced PINK1 protein level, whereas metformin did not influence in PINK1 protein level, and we also found ethanol and metformin did not influence on total PRKN level (Figure S2 AB). The mitochondrial lysate results show that PINK1 protein had a high expression on mitochondria in ethanol-treated samples, whereas metformin cannot influence PINK1 level in mitochondria (Figure 1 FG). Ethanol reduced the translocation of PRKN on mitochondrial, whereas metformin enhanced PRKN level on mitochondria (Figure 1 FG). We further used IF to confirm that ethanol inhibited mitochondria to recruit PRKN protein, whereas metformin can significantly increase the colocalization rates of PRKN and mitochondria (Figure S2 C).
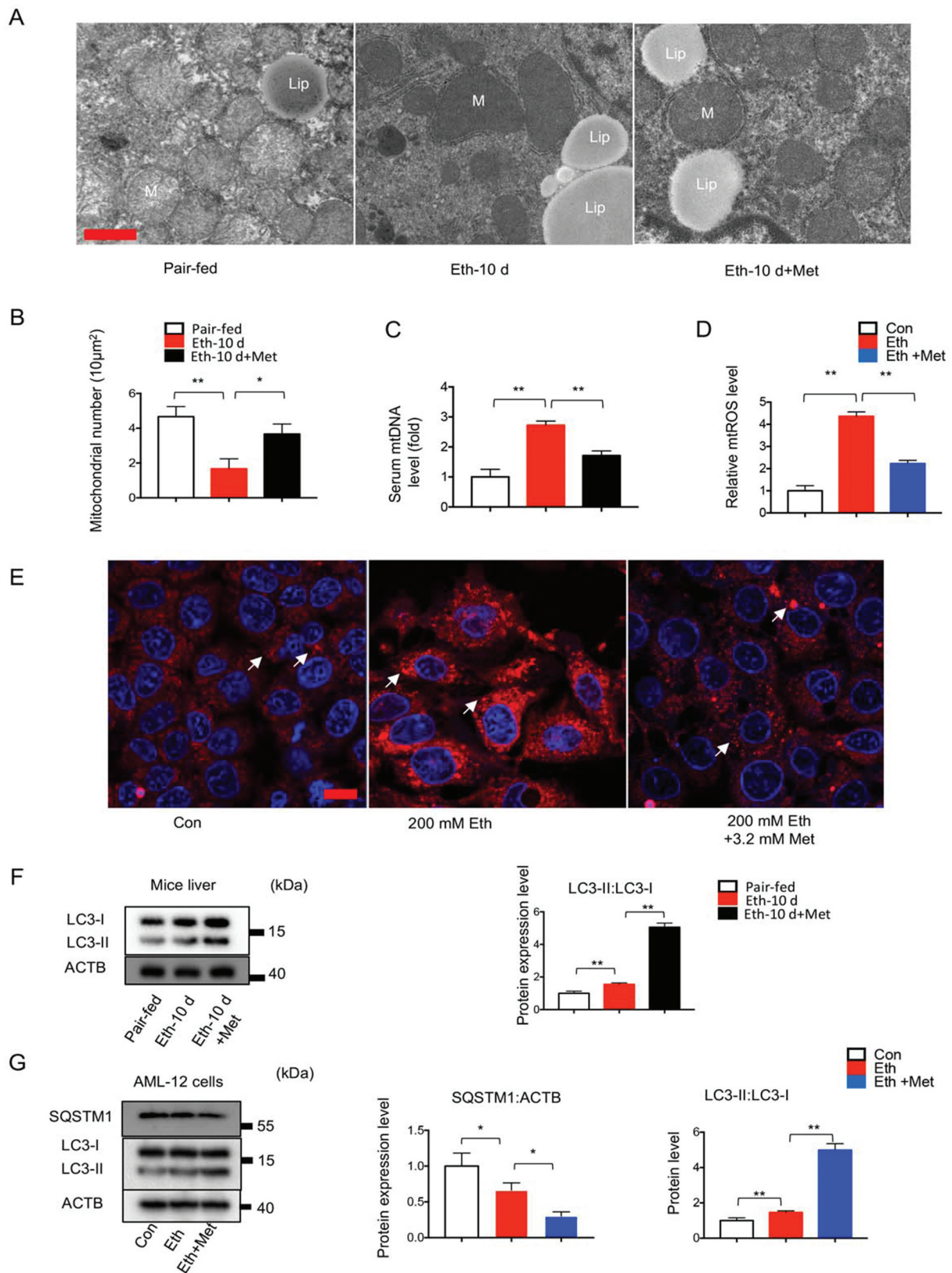
Figure 1. AMPK attenuates alcohol-induced liver injury and mitochondrial injury. (**A-C, F**) Analysis of mice on pair-fed mice (n = 15), 10-d eth-fed (n = 15), or treated with metformin at 150 mg/kg/day (Eth-fed+met, n = 15). (**D, E, G**) Analysis of AML-12 cells on control, 200 mM ethanol-treated for 24 h (Eth), 200 mM ethanol + 3.2 mM metformin-treated for 24 h (Eth+ Met). (A) Electron microscopy analyses of mice liver display mitochondria with normal morphology, destroyed cristae structure, and fewer mitochondrial number. (B) Quantification of mitochondrial number in 200 μm² (scale bar: 1 μm). (C) qRT-PCR was used to identify mtDNA level in mice serum, which can indicate mitochondrial injury level in mice hepatocytes. (D) AML-12 cells were stained with MTRC to identify the relative mtROS level. The fluorescence light intensity was measured by a multi-function micro reader. (E) AML-12 cells were stained with MTRC, and images were captured with a fluorescence microscope (scale bar: 50 μm) Arrow indicates mtROS points. (F, G) Western blot results show LC3-II:LC3-I ratio and SQSTM1 level in mice liver and AML-12 cells. ACTB was used as an internal reference in whole-cell lysates. Each experiment was repeated 3 times. Data are expressed as the mean ± SEM. * p < 0.05, ** p < 0.01.
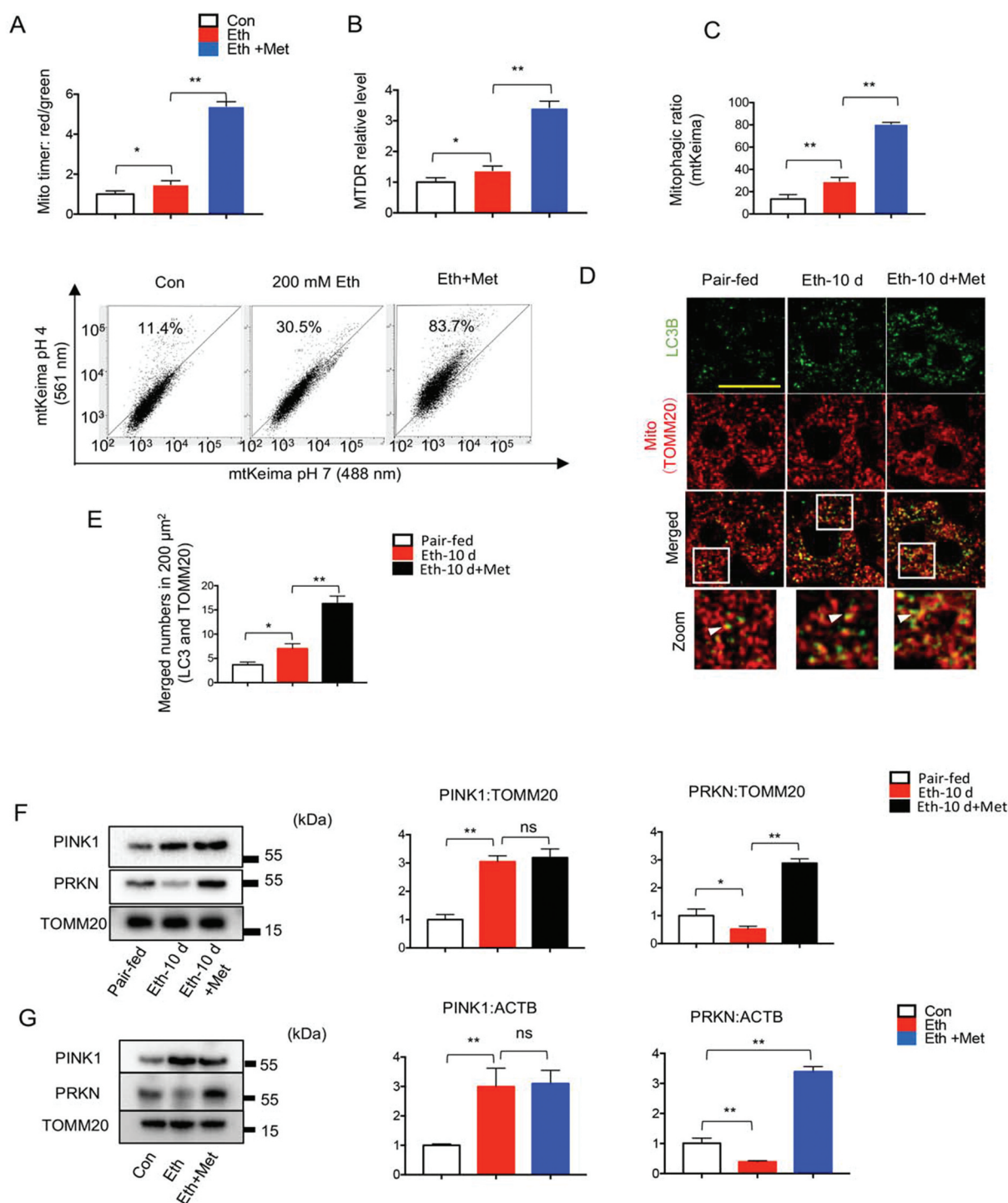
Figure 2. AMPK upregulates mitophagy level in mice and AML-12 cells. (**A-C, G**) Analysis of AML-12 cells on control, 200 mM ethanol-treated for 24 h (Eth), 200 mM ethanol + 3.2 mM metformin-treated for 24 h (Eth+ Met). (D-F) Analysis of mice on pair-fed mice (n = 15), 10-d eth-fed (n = 15), or treated with metformin at 150 mg/kg/day (Eth-fed+met, n = 15). (A) AML-12 cells were transfected with mito timer plasmid in advance (6 h), and were treated with ethanol, metformin (24 h). A multi-function micro reader was used to detect the 500:583 nm (green:red) fluorescence signal ratio. (B) AML-12 cells were treated with ethanol, metformin for 24 h, and were stained with MTDR for 15 min. A multi-function micro reader was used to detect 665 nm fluorescence light intensity. (C) FCM (flow cytometry) experiments and analysis. AML-12 cells were transfected with mtKeima plasmid in advance (6 h), and were treated with ethanol, metformin (24 h). Analysis of mitophagic ratio in Con, Eth, and Eth+Met cells. (D) IF staining results of mitochondria (TOMM20, red), LC3 (green) and nucleus (DAPI, blue) Scale bar: 10 μm. (E) Count of cells with LC3 on mitochondria (merged signal, yellow) in 200 μm^2. (F, G) Western blot results show the protein (PINK1, PRKN) level in mitochondrial lysates of mice livers and AML-12 cells. TOMM20 was used as an internal reference in mitochondrial lysates. Each experiment was repeated 3 times. Data are expressed as the mean ± SEM. * p < 0.05, ** p < 0.01.

In this study, we used metformin as an AMPK activator for *in vivo* and *in vitro* experiments. Metformin has many targets in cell signaling pathways. Hence, we also treated AML-12 cells with metformin and *Prkaa1* shRNA to confirm that metformin activates AMPK to attenuate ALD. Metformin significantly increased the p-AMPK level in AML-12 cells, whereas *shPrkaa1* can significantly inhibit total AMPK expression to reduce p-AMPK level (Figure S2 D). We also used MTRC to identify the mtROS level in cells, and we found that *shPrkaa1* can inhibit metformin protection in reducing ethanol-induced high mtROS level (Figure S2 E). The MTDR staining and western blot (LC3-II:LC3-I, SQSTM1) results also show that metformin enhanced mitophagy (including total autophagy) level in ethanol-treated cells, whereas *shPrkaa1* can significantly inhibit metformin-induced high mitophagy level (Figure S2 FG).

These experiments suggest that AMPK can significantly upregulate the mitophagy level in hepatocytes.

AMPK upregulates UQCRC2 protein level

Our experiments confirmed the correlation between AMPK and mitophagy. We wanted to find the downstream target of AMPK in ALD. According to WB, we found that ethanol reduced UQCRC2 protein expression in both animal and cell models, whereas metformin can significantly upregulate UQCRC2 protein level (Figure 3 AB). Interestingly, ethanol and AMPK did not influence other complex proteins (Figure 3 AB). In addition, we also used mitochondrial respiratory chain activity kits to confirm previous results. We found that ethanol inhibited complex III activity, and metformin can rescue its activity (Figure 3 CD). We also collected human samples and used IHC staining pictures to detect UQCRC2 protein levels. IHC results show that UQCRC2 protein significantly decreased in patient livers (Figure 3 E). Overall, we found that UQCRC2 protein level was inhibited in ALD, whereas AMPK may attenuate ALD via UQCRC2.

AMPK indirectly regulates UQCRC2 protein levels in ALD

The former figure suggested ethanol caused a low expression of UQCRC2 protein, and AMPK could significantly upregulate UQCRC2 protein level. Interestingly, qRT-PCR data showed that ethanol could not inhibit *Uqcrc2* gene level, whereas AMPK can enhance *Uqcrc2* gene level (Figure 4 A). Hence, we hypothesized AMPK might activate transcription factors to enhance the *UQCRC2* level. We then used RNA-seq to identify the transcription factor and found *Nfe2l2* was downregulated in model mice liver (Figure 4 BC). According to *UQCRC2* promoter analysis, there were three highly conserved response elements in the *UQCRC2* promoter, which NFE2L2 could bind (Figure 4 D); thus, we proposed that NFE2L2 functions as a transcriptional activator of *Uqcrc2*. Next, we performed a luciferase reporter assay driven by the *UQCRC2* promoter. Here, we demonstrated that NFE2L2 enhanced *Uqcrc2* gene expression (Figure 4 E). We used qRT-PCR to identify AMPK function on *Nfe2l2*, and observed that metformin treatments increased ethanol-induced low expression of *Nfe2l2* (Figure 4 F). According to

the ChIP binding qRT-PCR experiment, we found that the treatment of metformin can enhance *Uqcrc2* enrichment level in anti-NFE2L2, but no in the IgG group, whereas *shPrkaa1* can significantly reduce metformin-induced high *Uqcrc2* enrichment level in the anti- NFE2L2 group (Figure 4 G). Next, we used WB to identify the function of AMPK on NFE2L2. The blots showed that metformin could upregulate NFE2L2 protein level in AML-12 cells, whereas *shPrkaa1* can significantly reduce NFE2L2 protein level (Figure 4 H). Also, we found that UQCRC2 protein was inhibited in ethanol-treated cells, and metformin can upregulate UQCRC2 protein level, whereas *shNfe2l2* treatment can significantly inhibit UQCRC2 protein level in metformin and ethanol-treated cells (Figure 4 I). The *shNfe2l2* plasmid has high efficiency (Figure S3). All those experiments indicated that NFE2L2 is a crucial transcription factor in the regulating *UQCRC2*, and AMPK can activate NFE2L2. Consequently, in this study, we can confirm the AMPK-NFE2L2 axis to upregulate UQCRC2 protein.

The effects of UQCRC2 genetic intervention in mice and AML-12 cells

In this study, we selected a liver-specific AAV (adeno-associated virus) to KD (knock down) UQCRC2 protein in mice liver, and we also treated mice with lentivirus to overexpress (OE) UQCRC2. We chose plasmid to OE or KD UQCRC2 in AML-12 cells. The GPT and GOT1 level was not influenced by UQCRC2 OE or KD (Figure 5 AB), and the H&E (Figure 5 C) and oil red staining (Figure 5 D) pictures showed that UQCRC2 OE or KD could not change liver morphology and lipid accumulation level in control diet mice. The qRT-PCR data indicated that UQCRC2 OE or KD cannot change mtDNA level in serum (Figure 5 E). The MTRC staining results show that mtROS level was not changed after UQCRC2 genetic interventions (Figure 5 F). Interestingly, MTDR and mtKeima experiments showed that UQCRC2 OE may enhance mitophagic flux, whereas UQCRC2 KD significantly inhibits mitophagy (Figure 5 GH). The IF pictures show that UQCRC2 OE could enhance the colocalization rate of LC3 and mitochondria, whereas UQCRC2 KD inhibited mitochondria to recruit LC3 protein (Figure 5 I).

To further investigate the mitophagic flux, we detected LC3-II:LC3-I ratio, PRKN and PINK1 protein level in both mice and AML-12 cells. We found that UQCRC2 OE can enhance the LC3-II:LC3-I ratio, whereas UQCRC2 KD significantly inhibited LC3 activation (Figure 5 JK) (Figure S4 A). UQCRC2 KD and OE dramatically changes the level of LC3-II, suggesting that general autophagy (not only mitophagy) is impaired. We next used the starvation-induced autophagy model to identify the UQCRC2 function on autophagy. Firstly, we confirm that starvation (1% fetal serum) for 12 h could significantly induce high autophagy-flux (Figure S4 B). We then treated UQCRC2 KD cells with 1% fetal serum for 12 h. The following western blot results show that there is still a surge in UQCRC2 KD cells in autophagy-flux, and no significance was seen between UQCRC2 KD+starved and starved cells. (Figure S4 C) This evidence implicates that
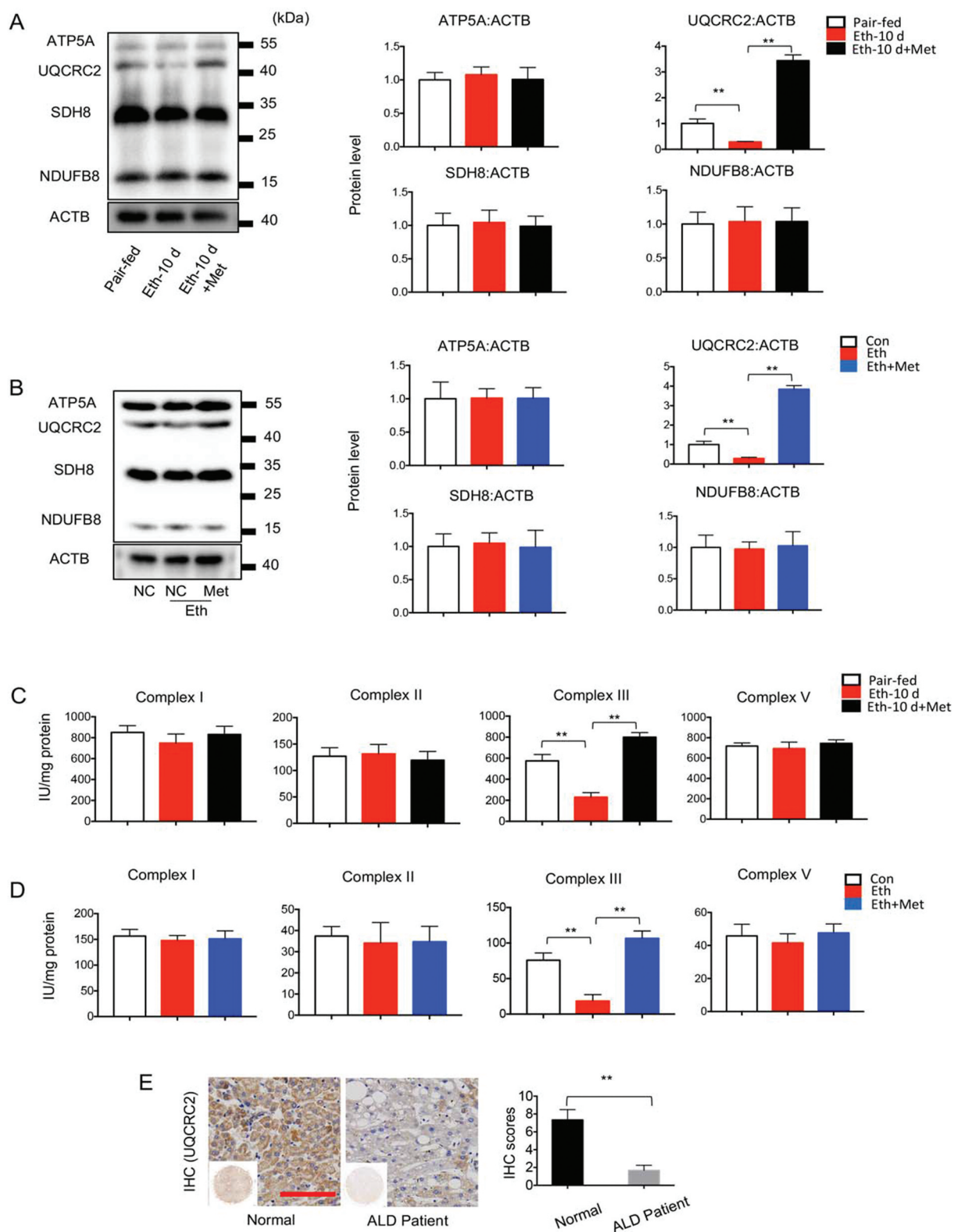
Figure 3. AMPK upregulates UQCRC2 protein level (Complex III activity) in ALD. (A, C) Analysis of mice on pair-fed mice (n = 15), 10-d eth-fed (n = 15), or treated with metformin at 150 mg/kg/day (Eth-fed+met, n = 15). (B, D) Analysis of AML-12 cells on control, 200 mM ethanol (Eth), 200 mM ethanol + 3.2 mM metformin (Eth + Met). (A, B) Western blot results: Ethanol caused the low expression of UQCRC2 protein in liver and AML-12 cells, whereas metformin can significantly enhance UQCRC2 protein level. (C, D) Mitochondrial activity assay: Ethanol reduced complex III activity, whereas metformin can upregulate complex III activity in 10 days ethanol-fed mice or ethanol-treated AML-12 cells. (E) IHC results of UQCRC2 in human samples, and IHC scores analysis. Each experiment was repeated 3 times. Data are expressed as the mean ± SEM. * p < 0.05, ** p < 0.01.

Figure 4. AMPK indirectly regulates UQCRC2. (A) qRT-PCR results of *Uqcrc2* mRNA fold in pair-fed mice (n = 15), 10-d eth-fed (n = 15), or treated with metformin at 150 mg/kg/day (Eth-fed+met, n = 15). (B) A heatmap showed differenti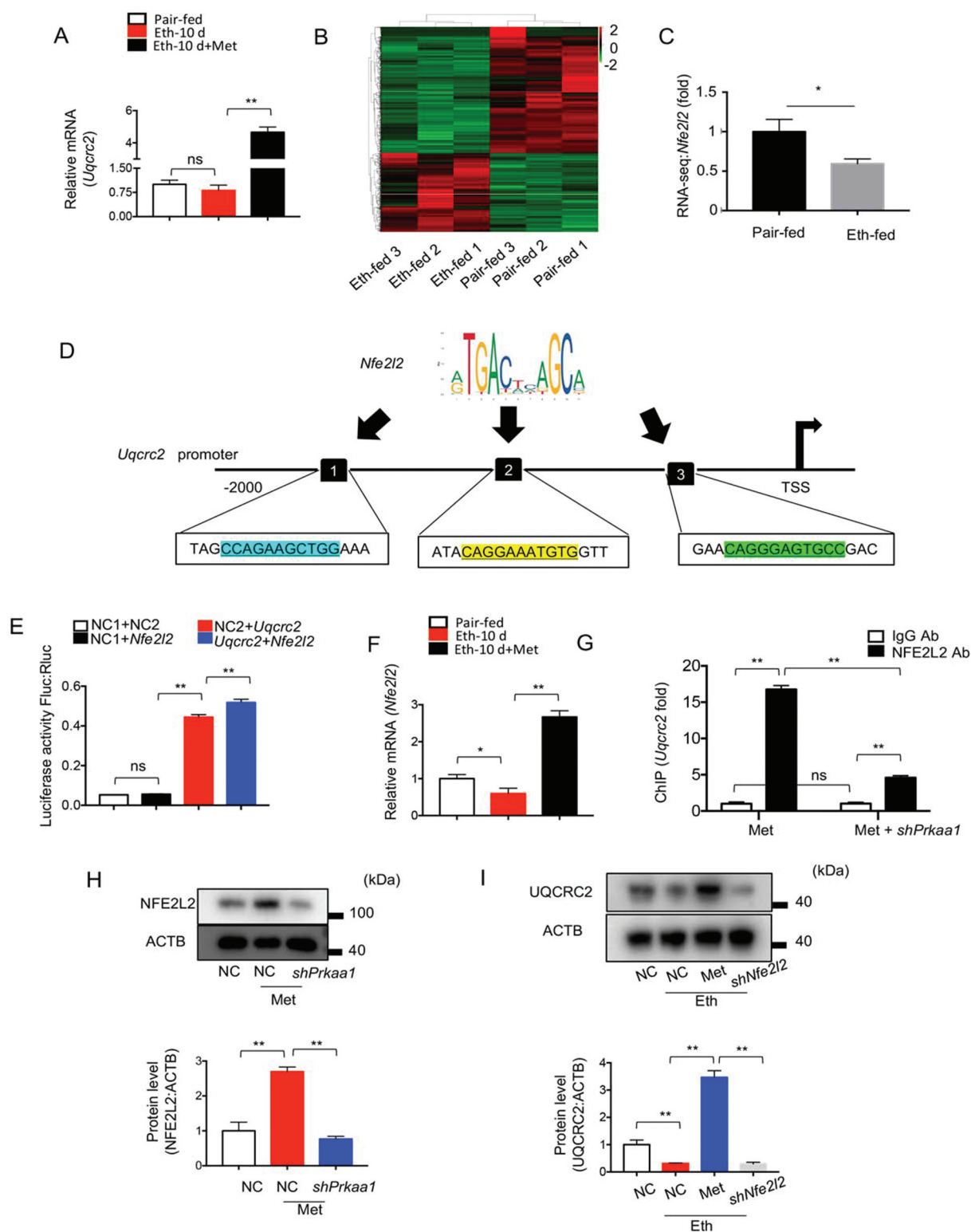ally expressed RNA with the same expression pattern in pair-fed and 10-d eth-fed mice. (C) *Nfe2l2* fold change (RNA-seq results). (D) Gene promoter analysis: Three sites in *Uqcrc2* promoter that NFE2L2 can bind. (E) Luciferase reporter gene results in AML-12 cells. AML-12 cells were transfected with NC$_1$ (pGL3-basic) + NC$_2$ (pcDNA3.1), NC$_1$+ pGL3-*Nfe2l2*, NC$_2$+ pcDNA3.1-*Uqcrc2*, pGL3-*Nfe2l2*+ pcDNA3.1-*Uqcrc2*. Data are presented as the ratio of Renilla luciferase activity to firefly activity (n = 3). (F) qRT-PCR results of *Nfe2l2* mRNA fold in pair-fed mice (n = 15), 10-d eth-fed (n = 15), or treated with metformin at 150 mg/kg/day (Eth-fed+met, n = 15). (G) ChIP assay showing the interaction of NFE2L2 with the potential binding site on the *Uqcrc2* promoter in AML-12 cells. Metformin enhanced UQCRC2 fold number in the anti- NFE2L2 group, whereas *shPrkaa1* reduced metformin-induced high enrichment of UQCRC2 in the anti-NFE2L2 group. (H, I) Analysis of AML-12 cells on NC (negative control), NC+ 3.2 Metformin (Met), 3.2 mM Met + *shPrkaa1* (50 nM), NC+ ethanol, NC+ethanol + metformin, Ethanol + Metformin + *shPrkaa1*. Western blot results show NFE2L2 and UQCRC2 protein levels in AML-12 cells. ACTB was used as an internal reference in whole-cell lysates. Each experiment was repeated 3 times. Data are expressed as the mean ± SEM. * p < 0.05, ** p < 0.01.
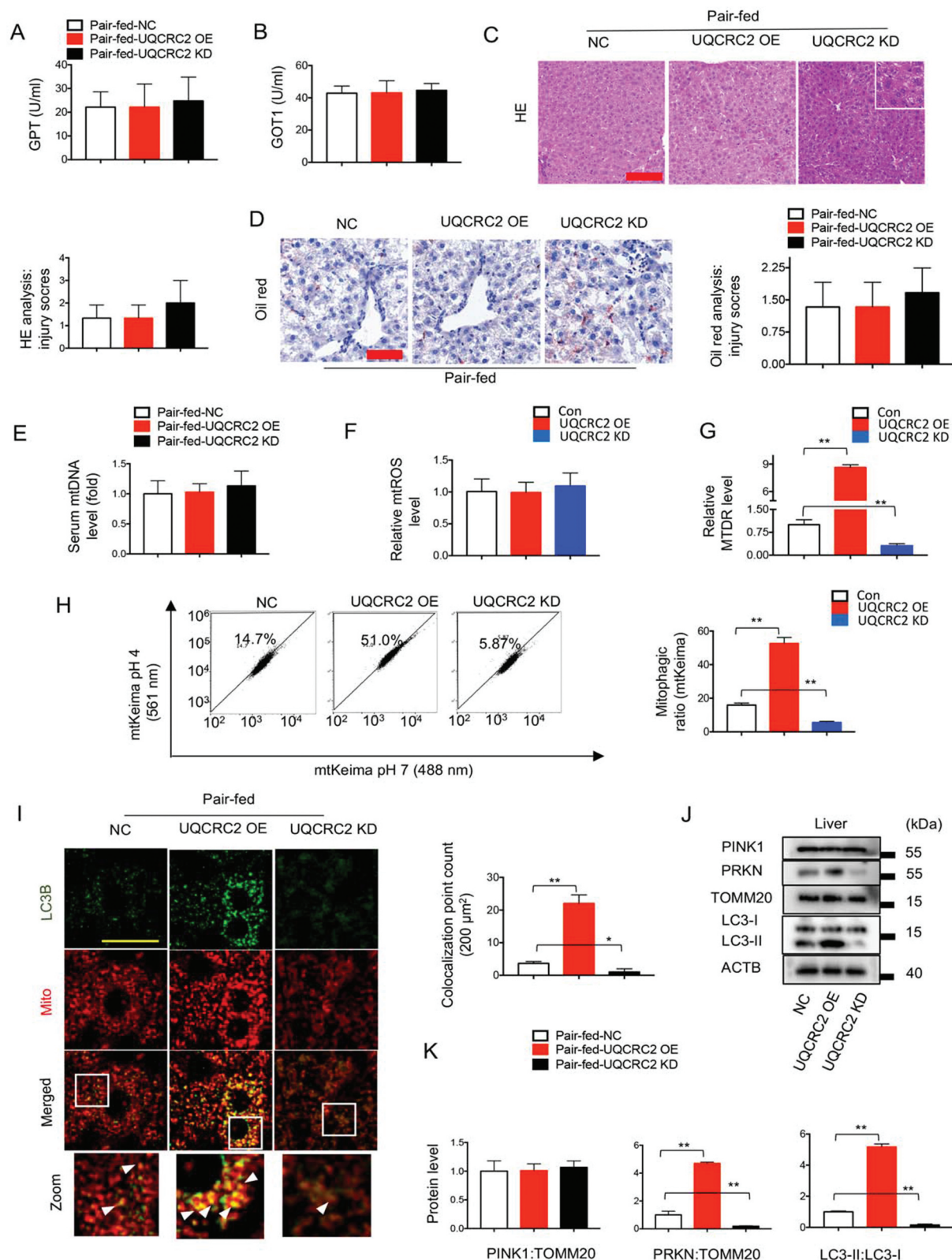
Figure 5. The effects of UQCRC2 genetic intervention in mice and AML-12 cells. (**A- E, I- K**) Analysis of mice on pair-fed mice was injected with AAV-NC or lentivirus-NC (n = 15), pair-fed mice were injected with AAV-UQCRC2 OE (n = 15), or pair-fed mice were injected with AAV-UQCRC2 KD (n = 15). (F-H) Analysis of AML-12 cells on NC plasmid (50 nM), UQCRC2 OE plasmid (50 nM), UQCRC2 KD plasmid (50 nM). (A, B) Test of GPT, and GOT1 levels in serum. (C) HE staining results and analysis: UQCRC2 OE or KD cannot cause liver injury (scale bar: 200 μm). (D) Oil red staining results and analysis: UQCRC2 OE or KD cannot influence lipid accumulation in mice liver (scale bar: 100 μm). (E). qRT-PCR was used to identify the mtDNA level in mice serum. (F) AML-12 cells were stained with MTRC to identify the relative mtROS level. The fluorescence light intensity was measured by a multi-function microplate reader. (G) AML-12 cells were treated with ethanol, metformin for 24 h, and were stained with MTDR for 15 min. A multi-function micro reader was used to detect 665 nm fluorescence light intensity. (H) FCM (flow cytometry) experiments and analysis. AML-12 cells were transfected with mtKeima plasmid in advance (6 h), and were treated with ethanol, metformin (24 h). Analysis of mitophagic ratio in NC, UQCRC2 OE, and UQCRC2 KD cells. (I) IF staining results of mitochondria (TOMM20, red), LC3 (green) and nucleus (DAPI, blue) Scale bar: 10 μm. Count of cells with LC3 on mitochondria (merged signal, yellow) in 200 μm². (J, K) Western blot results show the protein (PINK1, PRKN) level in mice livers. TOMM20 was used as an internal reference in mitochondrial lysates. WB results show LC3-II:LC3-I ratio in mice liver. ACTB was used as an internal reference in whole-cell lysates. Each experiment was repeated 3 times. Data are expressed as the mean ± SEM. * p < 0.05, ** p < 0.01.

UQCRC2 could only regulate mitophagy level. According to mitochondrial lysates results (western blot), we confirmed that UQCRC2 genetic treatment could not influence PINK1 protein level in mitochondria (Figure 5 JK) (Figure S4 D). Interestingly, the IF results helped us understand that UQCRC2 OE can enhance mitochondria translocation of PRKN protein, whereas UQCRC2 KD significantly inhibited its translocation (Figure S4 E1, E2). Interestingly, UQCRC2 genetic treatment did not influence the total expression of PRKN and PINK1 in the liver (Figure S4 F) and AML-12 cells (Figure S4 G).

UQCRC2 intervention regulates mitophagy in AML-12 cells

UQCRC2 is a critical protein in the mitochondrial respiratory chain, and genetic interventions would have a massive impact on electron transport chain (ETC) functions. Previous results did not identify whether the specific protein UQCRC2 is the central mediator of this pathway, or whether it is essentially "just" an indicator for a more or less general ETC dysfunction? All genetic interventions performed on UQCRC2 will have a massive impact on ETC function, ATP producing ratio, and thus AMPK activity. To clarify the role of UQCRC2 protein in mitophagy, we detected oxygen consumption rate (OCR), ATP, and mitochondrial membrane potential ($\Delta\Psi$). We found that OCR level was not changed in UQCRC2 KD cells comparing with control cells (Figure 6 A), whereas UQCRC2 KD treatment significantly reduced ATP producing rates (Figure 6 B) and $\Delta\psi$ (Figure 6 C). These results suggest that the UQCRC2 KD treatment has an uncoupling function, whereas no increasing mitophagy level was seen in UQCRC2 KD treated mice and AML-12 cells in the former Figure. Furthermore, we treated AML-12 cells with carbonyl cyanide 3-chlorophenylhydrazone (CCCP, a specific mitophagy agonist that can uncouple oxygen-consuming and ATP producing). The OCR and ATP experiments show that CCCP treated cells, and CCCP+UQCRC2 KD treated cells consumed more oxygen than control cells (Figure 6 D), whereas no ATP producing rates increase was seen in CCCP+UQCRC2 KD AML-12 cells (Figure 6 E). LC3 blots showed that CCCP caused high mitophagic levels in cells, whereas UQCRC2 KD significantly inhibited CCCP-induced high mitophagic flux (Figure 6 F). The western blot results also show that UQCRC2 KD caused a high p-AMPK level in AML-12 cells, whereas only a 1.5-fold increase was seen (Figure 6 G). To further investigate the correlations of UQCRC2 in PINK1-PRKN, we used *Pink1* siRNA plasmid to the knock down the PINK1 protein level, and we found that *Pink1* siRNA has high efficiency (Figure 6 H). We then used CCCP to activate mitophagy (PRKN translocation level). Interestingly, the western blots show that PINK1 KD could significantly inhibit PRKN translocation in CCCP treated cells, whereas UQCRC2 OE treatment could help PRKN translocate on mitochondria in PINK1-deficient cells (Figure 6 I). Overall, UQCRC2 genetic interventions regulate mitophagy.

UQCRC2 OE and KD can attenuate or deteriorate ALD through mitophagy

To investigate the function of UQCRC2 in ALD, we built the ALD mice model and cell model. UQCRC2 OE reduced alcohol-induced high GPT and GOT1 levels, whereas UQCRC2 KD enhanced alcohol-caused elevated GPT and GOT1 levels (Figure 7 AB). According to H&E (Figure 7 C) and oil red staining results (Figure 7 D), UQCRC2 OE attenuated alcohol-induced lipid accumulation, whereas UQCRC2 KD caused lipid accumulation in ethanol-fed mice severely.

We then focused on mitochondria. UQCRC2 OE reduced alcohol-induced high mtDNA level, whereas UQCRC2 KD significantly enhanced the mtDNA level in response to alcohol-fed for 10 days (Figure 7 E). The MTRC results show that UQCRC2 OE could attenuate ethanol-induced high mtROS level, whereas UQCRC2 KD enhanced the mtROS level in AML-12 cells (Figure 7 F). We further used MTDR staining (Figure 7 G), IF (LC3-mito) (Figure 7 HI), and mtKeima experiments (Figure 7 J) to identify the function of UQCRC2 KD or OE in ethanol-treated cells or mice. The results show that UQCRC2 OE significantly enhanced mitophagic flux, whereas UQCRC2 KD significantly inhibited mitophagy level. Furthermore, the WB show that UQCRC2 OE could upregulate LC3-II:LC3-I ratio in mice liver, whereas UQCRC2 KD inhibited LC3 activation (Figure 7 K). UQCRC2 OE can enhance PRKN expression level on mitochondria, whereas UQCRC2 KD significantly inhibited PRKN protein mitochondria translocation level (Figure 7 K). However, the WB also shows that UQCRC2 genetic interventions could not influence PINK1 protein level on mitochondria (Figure 7 K). Those experiments suggested UQCRC2 may regulate ALD through mitophagy.

UQCRC2 protein is required for AMPK regulating mitophagy in ALD

To investigate the function of UQCRC2 in AMPK protecting against ALD, we knocked down UQCRC2 both in mice and AML-12 cells, and built *in vivo* and *in vitro* ALD model.

Metformin can decrease ethanol-induced the high levels of GPT, GOT1 (Figure 8 AB), whereas the protective effects of metformin were partly inhibited in UQCRC2 KD mice fed to ethanol. The HE (Figure 8 C) and oil red staining (Figure 8 D) pictures also support that metformin can attenuate alcohol-induced lipid accumulation, whereas only a slight decrease was in UQCRC2 KD mice fed with ethanol after metformin treatment. Consequently, metformin still has protective effects in UQCRC2 KD mice in ALD.

We then focused on mitochondria. The qRT-PCR data indicate that metformin reduced ethanol-induced high mtDNA level in mice serum, whereas the protection of AMPK was not seen in UQCRC2 KD mice (Figure 8 E). We found that metformin reduced ethanol-induced high mtROS level, whereas metformin cannot reduce the high mtROS level in UQCRC2 KD mice fed to ethanol (Figure 8 F). According to MTDR (Figure 8 G), mtKeima (Figure 8 H), IF staining
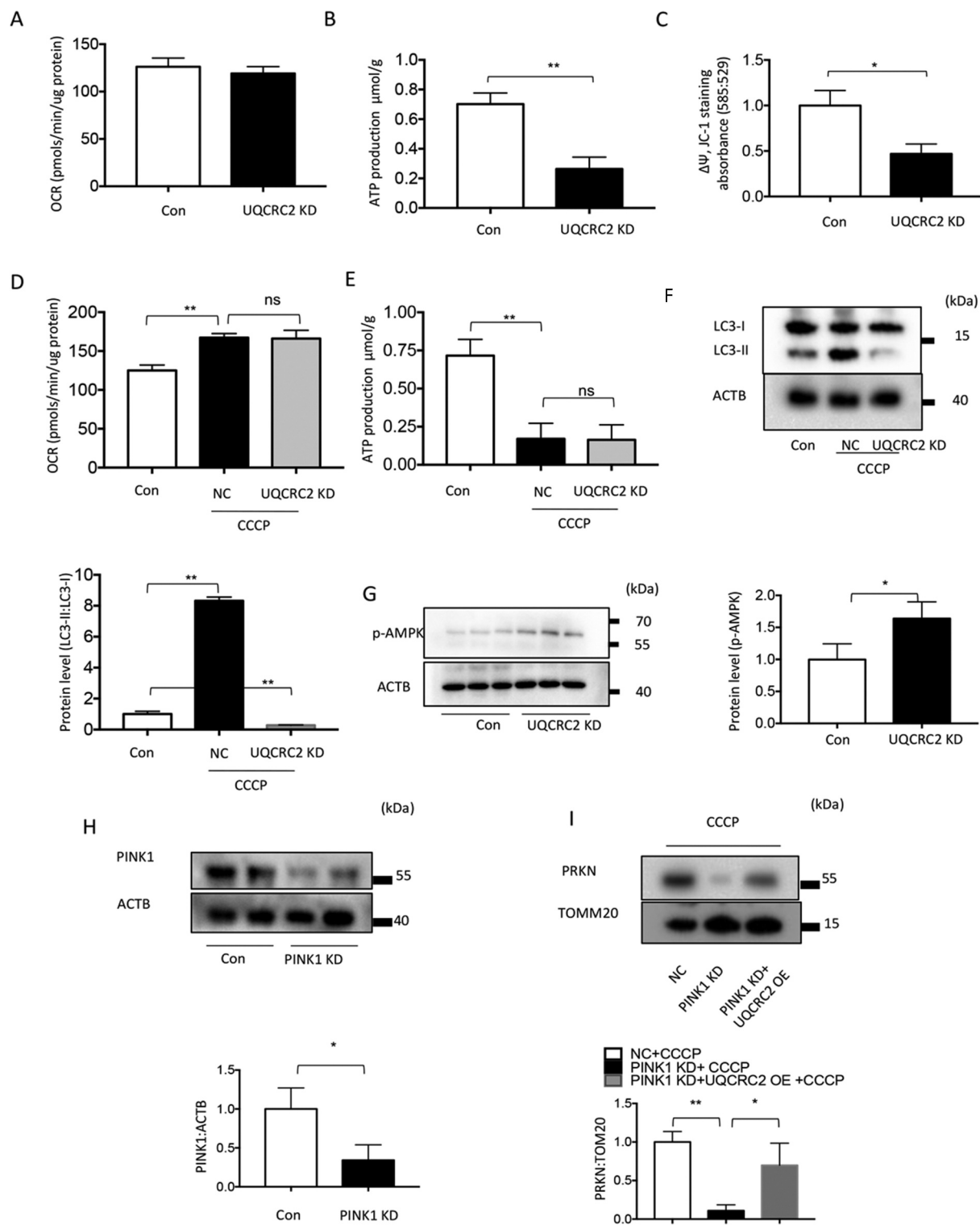
Figure 6. UQCRC2 intervention regulates mitophagy in AML-12 cells. (A) OCR in NC and UQCRC2 KD AML-12 cells. (B) ATP production level in NC and UQCRC2 KD AML-12 cells. (C) JC-1 staining results of NC and UQCRC2 KD AML-12 cells. The ratio of absorbance 585:529 is ΔΨ. (D) OCR in NC, 10 μM CCCP, and 10 μM CCCP+UQCRC2 KD AML-12 cells. (E) ATP production level in NC, 10 μM CCCP, and 10 μM CCCP+UQCRC2 KD AML-12 cells. (F) Western blot results show the LC3 II/LC3 I ratio in AML-12 cells. ACTB was used as an internal reference in whole-cell lysates. (G) Western blot results show the p-AMPK level in NC and UQCRC2 KD AML-12 cells. ACTB was used as an internal reference in whole-cell lysates. (H) Western blot results show the PINK1 level in NC and PINK1 KD AML-12 cells, (I) and PRKN protein level on mitochondria in NC+CCCP, PINK1 KD+CCCP, and PINK1 KD+ UQCRC2 OE+CCCP AML-12 cells. ACTB was used as an internal reference in whole-cell lysates. TOMM20 was used as an internal reference in mitochondrial lysates. Each experiment was repeated 3 times. Data are expressed as the mean ± SEM. * p < 0.05, ** p < 0.01.

(LC3-mito) (Figure 8 I), and WB (LC3-II:LC3-I, PRKN) (Figure 8 JK), we found that metformin enhanced mitophagy level in ethanol-treated cells, whereas metformin cannot

upregulate mitophagic flux in UQCRC2 KD mice fed with alcohol. The WB pictures also show that PINK1 was recruited to mitochondria in ethanol-treated hepatocytes, whereas
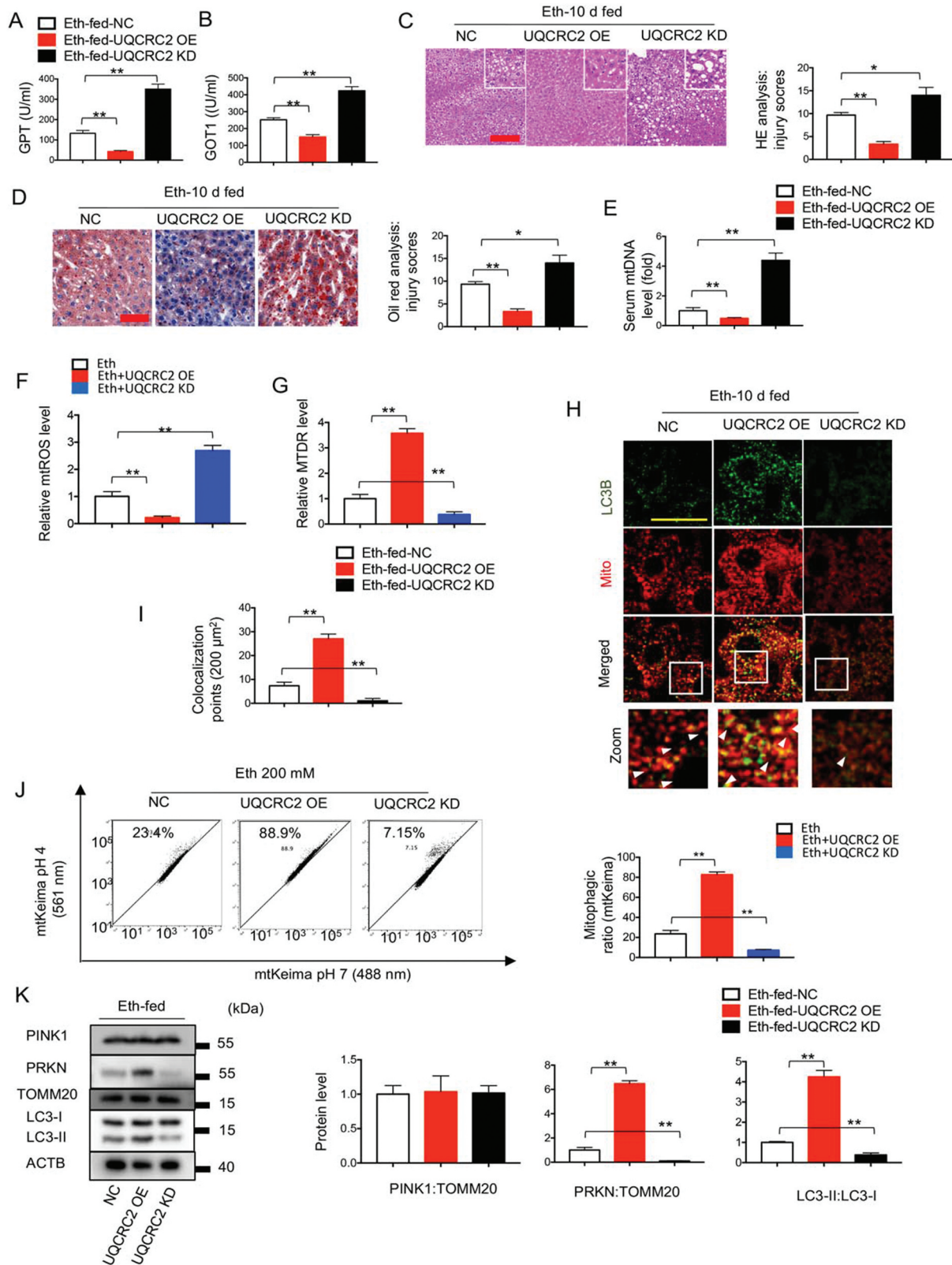
Figure 7. UQCRC2 OE or KD can attenuate or deteriorate ALD through mitophagy. (**A-E, H, I, K**) Analysis of mice on 10-d Eth-fed mice was injected with AAV-NC or lentivirus-NC (n = 15), 10-d Eth-fed mice were injected with AAV-UQCRC2 OE (n = 15), or 10-d Eth-fed were injected with AAV-UQCRC2 KD (n = 15). (**F, G, J**) Analysis of AML-12 cells on 200 mM Eth + NC plasmid (50 nM), Eth+ UQCRC2 OE plasmid (50 nM), Eth+ UQCRC2 KD plasmid (50 nM). (A, B) Test of GPT, and GOT1 level in serum. (C) HE staining results and analysis (scale bar: 200 μm). (D) Oil red staining results and analysis (scale bar: 100 μm). (E) qRT-PCR was used to identify the mtDNA level in mice serum. (F) AML-12 cells were stained with MTRC to identify the relative mtROS level. The fluorescence light intensity was measured by a multi-function micro reader. (G) AML-12 cells were treated were stained with MTDR for 15 min. A multi-function micro reader was used to detect 665 nm fluorescence light intensity. (H, I) IF staining results of mitochondria (TOMM20, red), LC3 (green) and nucleus (DAPI, blue) Scale bar: 10 μm. Count of cells with LC3 on mitochondria (merged signal, yellow) in 200 μm². (J) FCM (flow cytometry) experiments and analysis. AML-12 cells were transfected with mtKeima plasmid in advance (6 h), and were detected by FCM. Analysis of mitophagic ratio in NC+Eth, Eth+UQCRC2 OE, and Eth+UQCRC2 KD cells. (K) Western blot results showing the protein (PINK1, PRKN) level in mice livers. TOMM20 was used as an internal reference in mitochondrial lysates. Western blot results show LC3-II:LC3-I ratio in mice liver. ACTB was used as an internal reference in whole-cell lysates. Each experiment was repeated 3 times. Data are expressed as the mean ± SEM. * p < 0.05, ** p < 0.01.
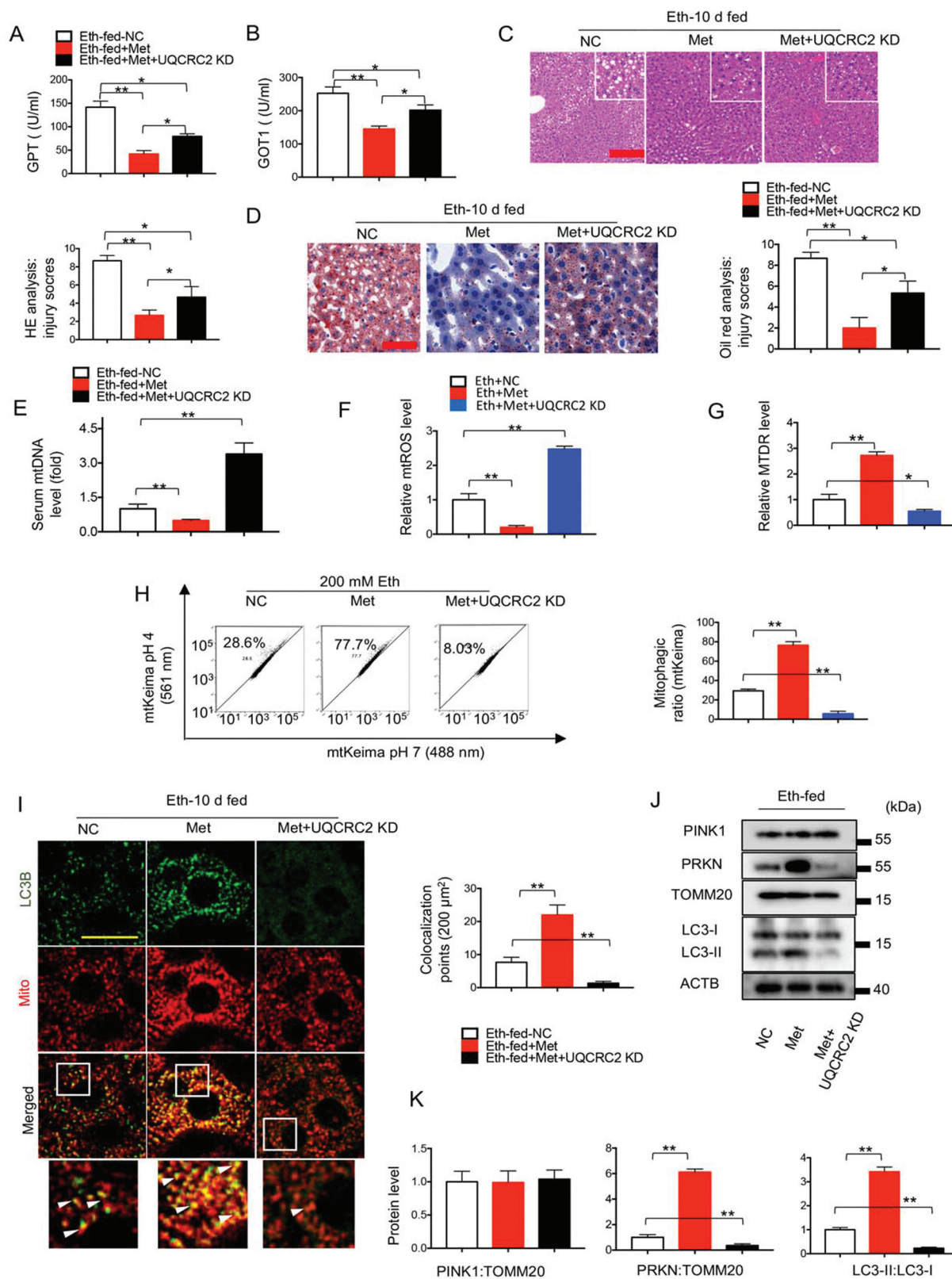
Figure 8. UQCRC2 protein is required for AMPK regulating mitophagy in ALD. (**A-E, I-K**) Analysis of mice on 10 d Eth-fed mice was injected with AAV-NC (n = 15), 10-d Eth-fed mice were orally administrated with 150 mg/kg metformin (n = 15), or 10-d Eth-fed were orally administrated with 150 mg/kg metformin and injected with AAV-UQCRC2 KD (n = 15). (F-H) Analysis of AML-12 cells on 200 mM Eth + NC plasmid (50 nM), Eth+ NC plasmid + 3.2 mM metformin, Eth+ UQCRC2 KD plasmid (50 nM) +metformin. (A, B) Test of GPT and GOT1 level in serum. (C) HE staining results and analysis (scale bar: 200 μm). (D) Oil red staining results and analysis (scale bar: 100 μm). (E) qRT-PCR was used to identify the mtDNA level in mice serum. (F) AML-12 cells were stained with MTRC to identify the relative mtROS level. The fluorescence light intensity was measured by a multi-function micro reader. (G) AML-12 cells were treated were stained with MTDR for 15 min, and were measured by a multi-function microplate reader. (H) FCM (flow cytometry) experiments and analysis. Analysis of mitophagic ratio in AML-12 cells. (I) IF staining results of mitochondria (TOMM20, red), LC3 (green) and nucleus (DAPI, blue) Scale bar: 10 μm. Count of cells with LC3 on mitochondria (merged signal, yellow) in 200 μm². (J, K) Western blot results showing the protein (PINK1, PRKN) level in mice livers. TOMM20 was used as an internal reference in mitochondrial lysates. WB results show LC3-Il:LC3-I ratio in mice liver. ACTB was used as an internal reference in whole-cell lysates. Each experiment was repeated 3 times. Data are expressed as the mean ± SEM. * p < 0.05, ** p < 0.01.

AMPK or UQCRC2 cannot influence its expression level (Figure 8 JK).

It has been reported that AMPK can regulate many signaling pathways [14,15]. Next, we identified whether UQCRC2 influenced beta-oxidation and lipogenic genes level (Figure S5 A). The qRT-PCR data shows that metformin reduced ethanol-induced high *Acaca* and *Fasn* levels, and metformin significantly upregulated alcohol caused low CPT1A and ACADM level. However, UQCRC2 KD cannot intervene in the protective effect of AMPK on *Acaca, Fasn, Cpt1a*, and *Acadm* genes level in mice. These results suggest UQCRC2 is not the target of AMPK in beta-oxidation and lipogenesis. Consequently, we understand why UQCRC2 KD cannot totally diminish AMPK protection in ALD.

A recent report highlighted adipose tissue function in NFALD. It suggests that insufficient AMPK may cause little mitophagy level in adipose tissue, and fatty acids may redirect to the liver, which caused fatty liver [16]. Consequently, the functions of AMPK and UQCRC2 in adipose tissue were needed to be identified. We chose 3T3-L1 cell line in this experiment. The MTDR staining results show that AMPK can significantly enhance mitophagic level, whereas UQCRC2 KD reduced mitophagic level (Figure S5 B). In addition, we also used WB to detect LC3-II:LC3-I ratio. The blots show that metformin activated LC3, whereas UQCRC2 KD inhibited LC3 activation (Figure S5 C).

Overall, those data suggest that UQCRC2 is an essential protein in AMPK regulating mitophagy, whereas UQCRC2 deficiency cannot totally inhibit the protective effects of AMPK in ALD.

PRKN protein is downstream of UQCRC2 in the mitophagy signaling pathway

Previous results suggest that UQCRC2 can recruit PRKN to mitochondria. To confirm the correlation of PRKN and UQCRC2 in ALD, we over-expressed PRKN in mice (Figure S6 A) and AML-12 cells (Figure S6 B). Firstly, we detected the GPT, and GOT1 levels in mice serum and discovered that high GPT, and GOT1 levels were seen in UQCRC2 KD mice fed with alcohol compared to only ethanol-treated mice, whereas PRKN OE can significantly reduce UQCRC2 KD and ethanol-induced high GPT, and GOT1 levels (Figure 9 AB). We then observed that *PRKN* OE significantly reduced the ethanol causes liver steatosis and fat accumulation in WT and UQCRC2 KD mice (Figure 9 CD).

Next, according to qRT-PCR (mtDNA) and MTRC staining, PRKN OE reduced ethanol-induced high mtDNA level and high mtROS level in WT and UQCRC2 KD mice/cells (Figure 9 EF). PRKN OE also overcame the inhibited effects of UQCRC2 KD in MTDR, which significantly increase MTDR fluorescence level (Figure 9 G). IF pictures indicate that PRKN OE can significantly increase the colocalization rates of LC3 and mitochondria in ethanol-treated UQCRC2 KD mice (Figure 9 HI). We further used western blot to detect LC3-II:LC3-I ratio to get quantification data. The blots show that UQCRC2 KD caused a low LC3-II:LC3-I ratio in ethanol-treated mice or cells, whereas PRKN OE can overcome the effects of UQCRC2 KD, and enhanced mitophagic flux significantly (Figure 9 J).

Overall, these results indicate that PRKN is the downstream protein of UQCRC2, and PRKN OE can rescue ethanol and UQCRC2 KD-induced mitochondria and liver injury.

Discussion

Mitochondria are important cellular organelles. Oxidation stress may damage mitochondria, thus resulting in the accumulation of injured mitochondria, which may lead to overproduction of ROS [6,12,17,18]. An insufficient number of mitochondria may also lead to excessive lipid and saccharide consumption [5,19,20]. Consequently, counting mitochondrial numbers cannot independently confirm the level of mitochondrial injury. In the current study, we used EM, mtROS, and mtDNA to identify mitochondrial injury levels. We also used the mito timer [6] and MTDR [21] to identify mitophagic flux. Interestingly, we found that MTDR was more sensitive than mito timer experiments and that MTDR experiments can also save time. Consequently, we chose MTDR in the following experiments. A previous study has indicated that mitophagy plays a crucial role in ALD, which helps reduce cellular senescence, inflammation, and accumulation of ROS and lipid oxidation [22]. Acute alcohol consumption is reportedly associated with a high level of mitophagy [20]. Another study indicated that chronic ethanol consumption suppresses lysosomal biogenesis and autophagy [5]. Our findings reveal that ethanol might induce a slight increase in mitophagy. According to our previous studies and other laboratory studies, radiation factors or additional injured stress can destroy mitochondria, while cells may not reach high enough mitophagy levels to protect themselves [8,22]. Thus, there exists a need to identify a better method to significantly upregulate mitophagy levels to attenuate liver injury.

AMPK is a classical metabolism-related target, which is well known for its ability to reduce inflammatory responses or metabolic disorders in liver disease [23,24]. However, to our knowledge, no report has uncovered the inner mechanism of AMPK involvement in mitophagy in ALD. In the present study, the mtKeima, LC3 (WB, IF), MTDR, and mito timer results showed that metformin significantly upregulated mitophagy levels and attenuated mitochondrial and liver injury. Interestingly, we found that p-AMPK levels were increased in ethanol-treated mice and cells. A previous report indicated that AMPK was activated in alcohol-induced liver disease [25]. Ethanol is a critical factor that causes liver injury, and can enhance p-AMPK levels. In a recent study, ROS could physiologically trigger AMPKs to protect cells in the initial stage [26]. Consequently, we hypothesized that the cell/liver protects itself in the early stage of liver injury by activating AMPK, whereas long-term oxidation can destroy the repair system (including the AMPK signaling pathway and autophagy). The long-term Binge mouse model helped us confirm that alcohol can induce a high p-AMPK level in the initial stage, whereas the p-AMPK level can be significantly inhibited in mouse livers after 2 months of alcohol treatment (Figure S1 G).

In typical pathways, researchers tend to focus on cardiolipin abnormity-induced mitochondrial dysfunction. The
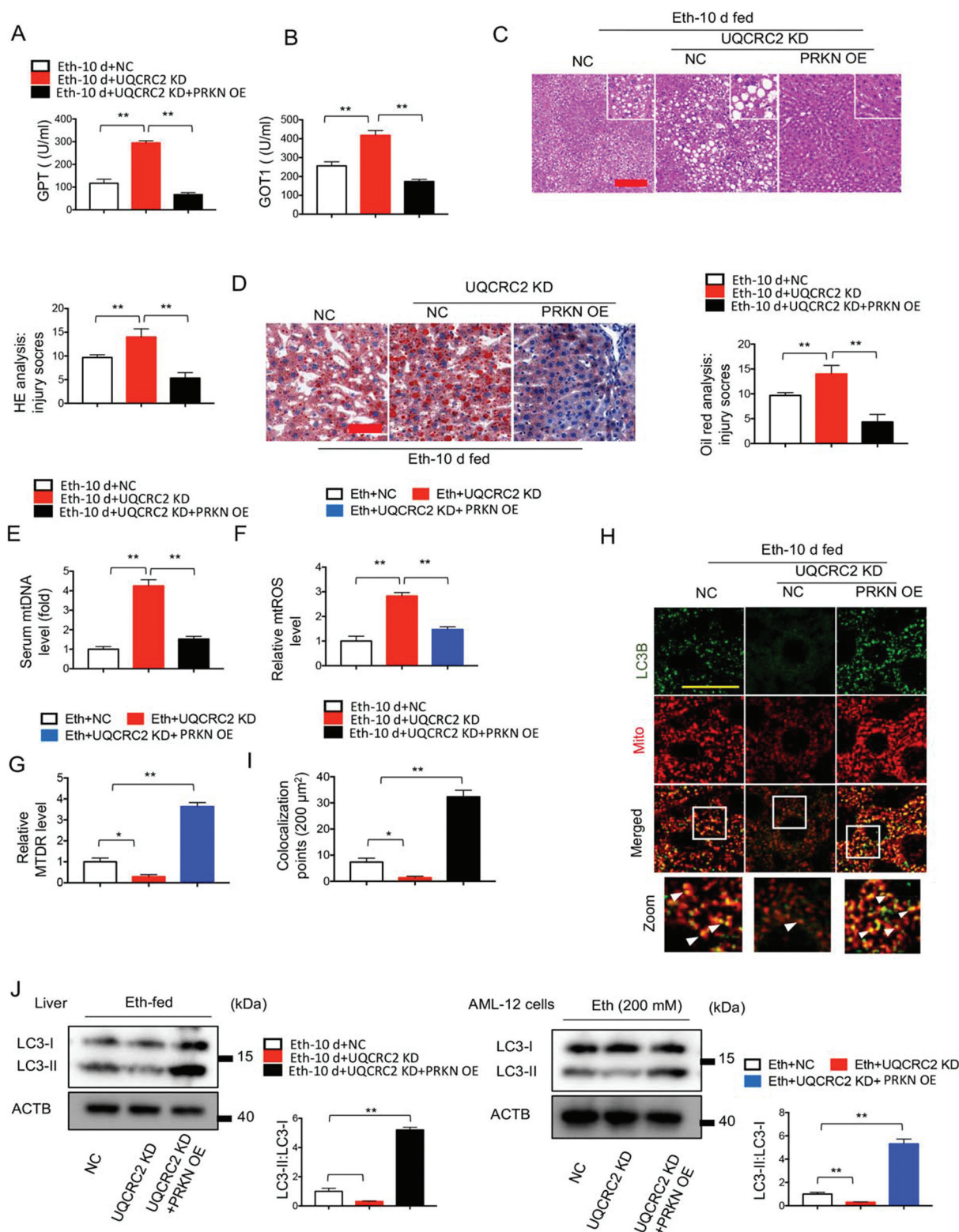
Figure 9. PRKN protein is downstream of UQCRC2 in the mitophagy signaling pathway. (**A-E, H-J**) Analysis of mice on 10-d Eth-fed mice was injected with AAV-NC (n = 15), 10-d Eth-fed mice were injected with AAV-UQCRC2 KD (n = 15), or 10-d Eth-fed mice were injected with AAV-UQCRC2 KD and AAV- PRKN OE (n = 15). (**F, G, J**) Analysis of AML-12 cells on 200 mM Eth, Eth+ UQCRC2 KD plasmid (50 nM) + PRKN OE plasmid (50 nM). (A, B). Test of GPT, and GOT1 level in serum. (C). HE staining results and analysis (scale bar: 200 μm). (D). Oil red staining results and analysis (scale bar: 100 μm). (E). qRT-PCR was used to identify the mtDNA level in mice serum. (F). AML-12 cells were stained with MTRC to identify the relative mtROS level. (G). AML-12 cells were treated were stained with MTDR for 15 min, and were measured by micro fluorescence reader at 665 nm. (H, I) IF staining results of mitochondria (TOMM20, red), LC3 (green) and nucleus (DAPI, blue) Scale bar: 10 μm. Count of cells with LC3 on mitochondria (merged signal, yellow) in 200 μm². (J). WB results show LC3-II:LC3-I ratio in mice liver and AML-12 cells. ACTB was used as an internal reference in whole-cell lysates. Each experiment was repeated 3 times. Data are expressed as the mean ± SEM. * p < 0.05, ** p < 0.01.
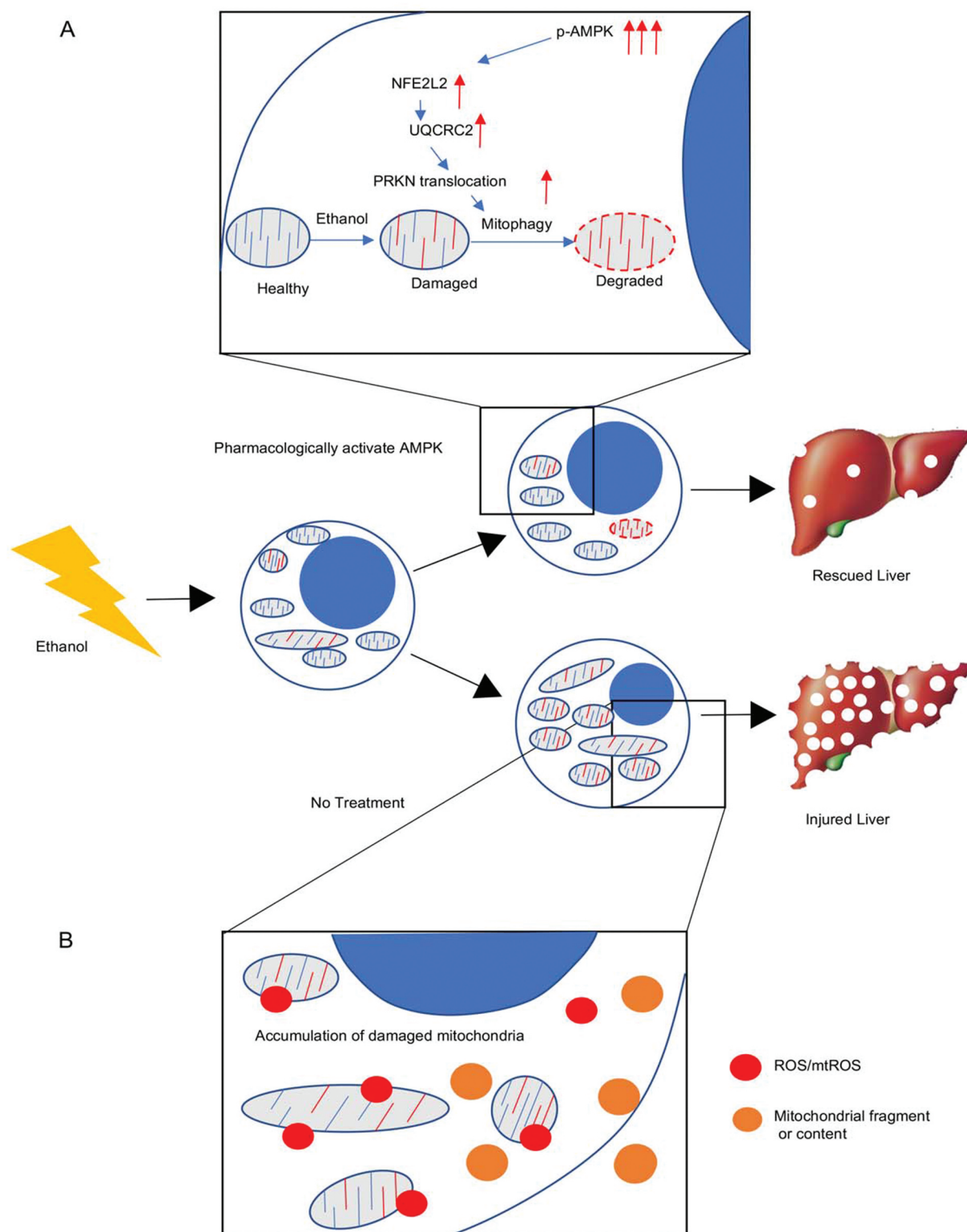
Figure 10. AMPK protects against ALD through the UQCRC2-PRKN axis. (A) In hepatocytes, AMPK enhances transcription factor (NFE2L2) level to increase UQCRC2 gene transcription. The ethanol-induced impaired mitochondria are degraded by the activated UQCRC2-PRKN axis. (B) Hepatocytes may develop more mtROS/ROS during ethanol treatment, and many mitochondria are destroyed, which mitochondrial fragments or content may dissociate in cell cytoplasm or serum.

phospholipid cardiolipin is an essential constituent of mitochondrial membranes and plays a role in several mitochondrial processes, including respiration and energy conversion [27]. Employing the RNAi method to knockdown cardiolipin synthase or phospholipid scramblase-3 may significantly inhibit mitophagy in cells [28]. However, a previous report also indicated that overload of cardiolipin may cause lung inflammation due to low expression of ATP8b1, a mitochondrial complex protein [29]. Cardiolipin is a critical marker of mitochondria [30], and plays key roles

in mitochondrial rebuilding. In this study, we confirmed that p-AMPK could upregulate mitophagy levels in ALD (Figure 2) and attempted to identify the target protein of AMPK in regulating mitophagy. In a previous report, a reduction in the phosphorylation of AMPK was found in diabetic encephalopathy. Dietary fish oil emulsion administration was shown to restore p-AMPK levels to preserve mitochondrial complex activity but was unable to prevent the shift toward saturated fatty acids in the cardiolipin composition [31]. This evidence suggests that AMPK regulates mitochondrial respiratory complexes in some diseases, but does not influence the cardiolipin pathway. Hence, we hypothesized that there exists another non-canonical pathway in ALD, in which a specific mitochondrial protein, which is regulated by p-AMPK, regulates mitophagy, whereas the content of cardiolipin serves just as an indicator of mitophagy level. Motivated by the need to conduct further research on the mitochondrial complex to understand the potential of mitochondrial proteins and identify which protein is critical in the mitochondrial respiratory chain, we studied the role of the mitochondrial complex in the pathogenesis of ALD in mice using western blotting and respiratory chain kits. Our results revealed that AMPK significantly upregulated an important subunit of the mitochondrial respiratory complex, UQCRC2, which is one of the 11 structural subunits of mitochondrial complex III. The main function of UQCRC2 is to transport electrons to the respiratory chain. Indeed, some studies have reported that the deficiency of mitochondrial complex III leads to neonatal-onset recurrent hepatocellular insufficiency, lactic acidosis, hypoglycemia, ketosis, and hyperammonemia [32]. Additionally, ubiquinone concentration was found to be severely reduced in mitochondria of *mfn2* (mitofusin 2) knockout hearts. MFN2 is an important player in the constant fusion-fission events necessary for the viability, normal distribution, and function of mitochondria [33]. These studies, as well as our results, suggest that UQCRC2 plays an important role in mitochondrial function and mitophagy, rather than only charging electron transport.

Recent studies have focused on transcription factors and PTMs (protein translation modifications) to identify indirect protein binding mechanisms [34]. We observed that the mRNA of *Uqcrc2* was unchanged in ethanol-induced injury livers, while UQCRC2 protein levels decreased in injured livers. UQCRC2 can be degraded by ubiquitylation [35,36], and ethanol can cause a high ubiquitylation level of protein [37]. The qRT-PCR results showed that AMPK significantly enhanced the *Uqcrc2* fold change numbers. Hence, we hypothesized that AMPK upregulates UQCRC2 expression in transcription and counteracts alcohol-induced protein degradation. Our previous study on pulmonary edema [38] confirmed that the transcription factor (NFE2L2) has a strong relationship with AMPK. Additionally, NFE2L2 plays a crucial role in autophagy and liver injury [39]. Hence, we utilized RNA-seq and bioinformatics to prove our hypothesis, and the data showed that NFE2L2 plays a critical role in ALD. We used promoter analysis, luciferase assay, ChIP, and WB to determine whether NFE2L2 is a transcription factor that enhances UQCRC2 fold change numbers, and briefly discuss the AMPK-NFE2L2 axis. In

typical pathways, researchers have focused on the effects of p-AMPK on NFE2L2 protein degradation. NFE2L2 nuclear translocation is strictly regulated by post-translational modifications of an adaptor protein of CUL3 (cullin 3)-based ubiquitin ligase KEAP1 and/or of an autophagy-specific substrate, namely SQSTM1, and KEAP1 and SQSTM1 are modulated by p-AMPK [40] Consequently, activated AMPK may help reduce NFE2L2 protein degradation. However, recent reports have indicated that AMPK can activate GSK3B (glycogen synthase kinase 3 beta) [41]. GSK3B can positively regulate NFE2L2 transcription [42]. Furthermore, a report indicates that LGALS1 (galectin 1) could attenuate LPS-induced lung injury via AMPK-NFE2L2 because LGALS1 could activate AMPK to enhance *Nfe2l2* gene expression [43]. Our results showed that *Nfe2l2* mRNA was low in the ethanol-treated group (Figure 4 B.C.F), and p-AMPK could upregulate *Nfe2l2* mRNA levels (Figure 4 F). These results suggest that ethanol could attenuate NFE2L2 transcription, and p-AMPK could regulate *Nfe2l2* mRNA. Although it cannot be excluded from the functions of AMPK in regulating PTMs of the NFE2L2, which inhibit the degradation (ubiquitination or autophagy) of NFE2L2 in ALD. It is worth noting that inhibiting ubiquitin or autophagy levels has had little success in ALD therapy because reducing NFE2L2 degradation could only restore NFE2L2 protein to normal levels at most, whereas cells with normal NFE2L2 levels cannot trigger the high mitophagy levels required to protect themselves. In contrast, our data suggest that p-AMPK-*NFE2L2* transcription may represent a possible strategy to enhance NFE2L2 protein levels as the treatment requires.

In non-alcohol-fed mice, UQCRC2 KD or OE did not change liver morphology, and UQCRC2 KD did not cause liver injury. Additionally, our data showed that UQCRC2 OE attenuated alcohol-induced lipid accumulation and liver injury, whereas UQCRC2 KD deteriorated the destructive function of alcohol in the liver. The mtKeima, LC3, MTDR, and mito timer results indicated that UQCRC2 significantly regulated mitophagy levels. Hence, we confirmed that UQCRC2 is the mitophagy-triggering protein, whereas deficiency of UQCRC2 cannot induce liver injury because alcohol is a critical factor in the production of oxidative stress [44]. UQCRC2 is a critical protein of the mitochondrial respiratory chain, and genetic intervention causes changes in ETC function. Thus, we attempted to clarify whether ETC function changes caused mitophagy due to UQCRC2 genetic intervention, or whether UQCRC2 protein can directly regulate mitophagy. Interestingly, we found that UQCRC2 KD reduced ATP:OCR ratio and ΔΨ. Reportedly, a low ratio of ATP: OCR and Δψ may induce mitophagy [45,46]. However, our previous IF and mtKeima data showed that UQCRC2 KD inhibited mitophagy. Furthermore, we confirmed that CCCP (a mitophagy agonist [8]) significantly induced mitophagic flux, whereas UQCRC2 KD inhibited CCCP-induced high mitophagy levels in AML-12 cells. These data helped us understand that UQCRC2 can independently regulate mitophagy, rather than indicating general ETC dysfunction.

PRKN, a core mitophagy-regulating protein, is recruited to damaged and depolarized mitochondria and induces

mitochondrial clearance [7]. PRKN deficiency, or little mitochondrial translocation, may inhibit mitophagy and is harmful to mice [5,47–49]. In typical pathways, PINK1, a neuroprotective protein mutated in autosomal recessive Parkinson disease, has been implicated in the activation of mitophagy by selectively accumulating on depolarized mitochondria and promoting PRKN translocation to them [50], and it has also been reported that two Ser residues (Ser228 and Ser402) in PINK1 are imperative for recruiting PRKN [51]. Recent reports indicated that PRKN could translocate to mitochondria independent of PINK1. Miro protein may help directly phosphorylate PRKN and recruit PRKN to mitochondria in PINK1-deficient cells [52]. Additionally, HSPA1L and BAG4 co-regulate PRKN localization following mitochondrial damage. HSPA1L knockdown in HeLa cells led to a significant decrease in parkin translocation, and BAG4 knockdown enhanced parkin translocation. Neither of these knockdowns affected the level of PINK1 protein accumulation [53]. In the present study, we also found high PINK1 protein enrichment in the mitochondria of ethanol-treated cells/liver and low PRKN protein levels in the mitochondria of ethanol-treated cells/liver (Figure 2 F). This suggests that PINK1 protein may not completely regulate PRKN protein in such a model, and there may be non-canonical pathways. Additionally, we confirmed that UQCRC2 OE significantly upregulated the Parkin protein level in mitochondria, whereas no influence was seen in the PINK1 protein (Figure 5 J). Furthermore, we used siRNA to knock down PINK1 protein in AML-12 cells. PINK1 KD treatment can significantly inhibit PRKN from translocating to mitochondria, whereas UQCRC2 OE treatment could help mitochondrial recruit PRKN protein (Figure 6 I). These results suggest that UQCRC2 can regulate PRKN translocation independent of PINK1. While recent studies [52,53] and our study highlight the beneficial effects of UQCRC2, miro, HSPA1L, or BAG4 in regulating PRKN translocation, the function of PINK1 in mitophagy remains undeniable. In contrast, the non-canonical pathways may offer a new choice in regulating mitophagy, in which UQCRC2 may function as a new switch that accelerates PRKN recruitment to mitochondria with or without PINK1 when cells undergo mitophagy dysfunction.

In this study, we also treated UQCRC2 KD mice/cells with metformin to verify the correlation between UQCRC2 and AMPK. Previous experiments have shown that UQCRC2 is a target of AMPK. Interestingly, HE, oil red, and GPT results showed that AMPK attenuated alcohol-induced liver injury in UQCRC2 KD mice, whereas AMPK did not upregulate mitophagy levels in UQCRC2 KD mice fed with alcohol. Some studies have indicated that AMPK can attenuate NAFLD by restricting de novo lipogenesis [54], enhancing fatty acid oxidation [55], and upregulating mitophagy levels in adipose tissue [56]. Hence, we hypothesized that UQCRC2 is a mitophagy regulator, whereas UQCRC2 KD does not influence fatty synthesis and beta-oxidation function in ALD. The qRT-PCR analysis supported our hypothesis that AMPK can reduce *Acaca, Fasn*, and enhance *Cpt1a* and *Acadm* gene level, whereas UQCRC2 KD did not influence these gene fold change numbers. Reduction of AMPK in adipose tissue reduces mitophagy, which leads to compromised white and brown adipose tissue mitochondrial function [57]. In white adipose tissue, this effect compromises ATP synthesis. It reduces the storage capabilities of this tissue, ultimately leading to fatty acids re-directed to peripheral tissues, such as the liver (fatty liver). We confirmed that AMPK activated mitophagy levels in 3T3-L1 cells, whereas UQCRC2 KD inhibited high metformin-induced mitophagy levels.

Conclusions

AMPK protects the liver against alcohol-induced liver injury via UQCRC2 to upregulate mitophagy (Figure 10). These findings highlight the mechanisms of transcription in ALD pathogenesis. They also provide the rationale for a key, specific, and therapeutic target via the pharmacological activation of UQCRC2 in the amelioration of the progression of this complex, debilitating disease.

Materials and methods

Clinical samples

An ALD tissue microarray containing 12 cases of ALD and paired adjacent normal tissue was purchased from Alenabio Biotech (LV248). Informed consent in writing was obtained from patients. This study protocol conformed to the ethical guidelines of the 1975 Declaration of Helsinki Principles. All samples were correctly labeled, clinically, and pathologically.

Genetically modified animal

Eight-week-old male C57BL/6 J mice (23 g) were purchased from the Nanjing Model Animal Research Institute. Adult mice were caudal vein injected with adeno-associated virus (AAV) (UQCRC2 KD, Hanbio, HH20180710WY-AAV01; PRKN OE, Hanbio, HH20181127WY-AAV01) vectors (3×10^{11} per mouse) expressing GFP-tagged or lentivirus (UQCRC2 OE; Genepharm, B7249) vectors (5×10^{7} per mouse) expressing GFP-tagged for 3 weeks. Mice injected with AAV vector or lentivirus vector were used as wild type (WT). The efficiency was detected by western blotting.

ALD mice model (Binge mice model)

The mice (WT or genetically modified) were fed with ethanol, according to the National Institute on Alcohol Abuse and Alcoholism (NIAAA) protocol (GOLD) [58]. All mice were fed in the Anhui Medical University in the vivarium facility with a 12-hour light/12-hour dark cycle (light on at 6:00 am). In this protocol, mice were given a liquid diet for 5 days for adaption and 10 days for ethanol feeding. The ethanol liquid diet comprised a 5% ethanol mixture. During the last day, the mice were treated with a lot of alcohol by gavage. The mice were euthanized after the ethanol gavage. The liver tissues were soaked in 4% paraformaldehyde or stored at −70°C.

For the long-term feeding, the same protocol was followed with the previously described (10 days ethanol feeding). In addition, mice were fed for 8 weeks with multiple binges

(twice a week) of ethanol (5 g/kg) feeding as described previously.

All animal experiments were performed after obtaining permission from the Ethics Committees of Anhui Medical University. All procedures were following accordance with the Guidelines of the Animal Care and Use Committee of Anhui Medical University.

Administration of metformin

Metformin (250 mg/kg; Selleck, S1950) was dissolved in saline, and was injected via oral gavage into the conscious mice 24 h prior to first time ethanol-fed, which was repeated daily until 10 days ALD model completed.

Cell transfection

AML-12 and 3T3-L1 cells were purchased from ATCC (CRL-2254, CL-173). Characterized AMPK KD, UQCRC2 KD or OE, NFE2L2 OE or KD, and PINK1 KD cells were used for this study. UQCRC2, NFE2L2-expressing plasmid (50 nM) or control pcDNA empty vector (Genepharm, 20,202,589) were transfected into AML-12/3T3-L1 cells by using Lipofectamine 2000 (Thermo Fisher Scientific, 11,668,019). Furthermore, The PRKAA1/AMPKα1 KD, UQCRC2 KD, and NRF2 KD cells were transfected with shRNA plasmid (50 nM) by using Lipofectamine 2000. The sequence of shRNA targeting mouse *Prkaa1, Uqcrc2, Nfe2l2* are as follows 1. *Prkaa1*: Forward: 5′-CACCGCACGAGTTGACCGGACATAATTCAAGAGATTA-TATGTCCGGTCAACTCGTCTTTTTTG-3′, Anti: 3′-GATCCAAAAAAGCACGAGTTGACCGGACATAATCTC TTGAATTATGTCCGGTCAACTCGTGC-5′, 2. *Uqcrc2*: Forward: 5′- CACCGCT GCGTCTTACATCCAGTCTCGAAAGACT GGATGTAAGACGCAGC-3′, Anti: 3′- CGACGCAGAATGT-AGGTCAGAGCTTTCTGACCTACATTCTGCGTCGAAAA-5′ 3. *Nfe2l2*: Forward: 5′-CACCGCAGGACATGGATTTGATTG-ATTCAAGA GATCAATCAAATCCATGTCCTGCTTTTTTG-3′, Anti: 3′-GATCCAAAAAAGC AGGACATGGATTTGATT-GATCTCTTGAATCAATCAAATCCATGTCCTGC-5′. The PI-NK KD cells were transfected by the si-*Pink1* plasmid. The sequence of si-PINK1 is as: Forward: 5′-GCUUCCGUCUGGA-GGAUUA-3′, Anti: 3′- UAAUCCUCC AGACGGAAGC-5′, and the si-control sequence is as: 5′-GCUUGCGU CGAGAGUCU-UA-3′, Anti: 3′- UAAGACUCUCGACGCAAGC-5′. In addition, we get PRKN OE AML-12 cells using AAV vectors (20 particles per cell).

Furthermore, AML-12 cells were also transfected with 50 nM mtKeima and mito timer plasmid for mitophagic flux detection. These two plasmids were purchased from Genepharm company.

Cell culture

AML-12 cells were grown in DMEM supplemented with 10% FBS, penicillin (100 U/mL) and streptomycin (100 μg/mL), and then were infected with 50 nM plasmid (PRKAA1 KD, UQCRC2 KD or OE) or PRKN OE AAV. After gene transfection, AML-12 cells were treated with 200 mM ethanol (200 mM) or 3.2 mM metformin for 24 hours for ALD *in vitro*

model. In addition, 3T3-L1 cells were grown in DMEM supplemented with 10% FBS, penicillin, and streptomycin. For other experiments, AML-12 cells were also treated with CCCP (MCE, HY-100,941; 10 μM), as shown in figure legends.

mtROS, mito timer, JC-1, and MTDR fluorescence detection

In this study, a multi-function microplate reader (Molecular Devices, ID3) was used to detect fluorescence intensity, and it can get accurate data as well as Flow cytometry.

The fluorophore MitoTracker Red CMXRos (MTRC, ex/em maxima ~ 580/600; Life Technologies, M7512) was used to detect the mitochondrial ROS to monitor mitochondrial injury. Treated (transfection or ethanol) cells were stained with 200 nM MTRC for 15 min before measurement.

JC-1 (em: 585 red, 529 green; Med Chem Express, HY-15,534) is a cationic fluorescent dye that enables the quantification of mitochondrial membrane potential.

Cells were transfected with a pTRE-tight-MitoTimer plasmid (50 nM) to detect mitochondrial renew rate in order to detect mitophagic flux. The mitophagic ratio was calculated by green:red (em maxima:514:639).

In addition, we also used MitoTracker Deep Red (MTDR: ex/em maxima ~ 644/665; Life Technologies, M22426) to detect the new synthesized mitochondrial. Cells were stained with 200 nM MTDR for 15 min before measurement.

Flow cytometry analysis

For the mtKeima assay, cells were pre-treated with 50 nM mtKeima plasmid or other gene transfection for 6 h, and treated with ethanol for 24 h. Cells then were trypsinized and resuspended in 1 ml chilled PBS (Hyclone, SH30256.01). The cell suspensions were held on ice and measured with a flow cytometry (Beckman counter, FC600). Events were preselected for viable, single-cell populations, which show excitation at 405 and emission at 610/620 nm. Fluorescent cells (10,000 per sample) were collected and analyzed for dual-excitation at 488 (pH 7) and 561 (pH 4) nm with 582/515 and 610/620 nm emission filters, respectively. By analysis of the 561 nm:488 nm ratio, the percentage of lysosomal mtKeima can be calculated. Data processing was done with FlowJo (v10, Tree Star).

Oxygen consumption rate (OCR) and ATP production rate

AML-12 cells were transfected with *shUqcrc2* for 24 h, and was given CCCP for 2 h at a concentration of 10 mM prior to measurement. OCR was measured using Extracellular O_2 Consumption Assay (Abcam, ab197243). ATP was also measured through an ATP Content Assay Kit (Solarbio, BC0305) following the manufacturer's instructions. AML-12 cells were seeded onto 96-well plates before the experiment. After treatment, cells were ultrasonic disruption, and lysates were centrifuged at 800 × g for 10 min at 4°C, the supernatant was collected for detection. To detect ATP level, the content of phosphocreatine was determined by the colorimetric method of phosphomolybdic acid at 700 nm. The protein

concentration of supernatant used in OCR and ATP assay was determined by the BCA Protein Assay kit (Solarbio, PC0020).

Histomorphology

The liver tissues were fixed with 4% paraformaldehyde and embedded in paraffin for histopathological examination. Liver tissues were sectioned into 5-μm sections using a rotary microtome (Leica). Sections were stained with hematoxylin and eosin (Solarbio, G1120). Five randomly selected ×200 fields per slide were photographed in a blinded manner.

Oil red staining

Liver tissues were isolated from mice after euthanasia and stored in 20 g•L-1 sucrose (Sigma, V900116) solution for no longer than 48 h. The frozen section procedures were as follows. Step 1: tissues were placed in 20 g•L^{-1} sucrose solution and OCT embedding solution (SAKURA, 4583) for 2 h at room temperature and a mixing ratio of 1:1. Step 2: tissues were placed in fresh OCT embedding solution for 4 h. Step 3: tissues were placed in fresh OCT embedding solution for 6 h. Step 4: tissues were placed on a frozen microtome to obtain tissue slices (glass slides) and frozen tissues.

The sections furthermore were stained with oil red kits (Solarbio, G1261). The brief procedures were as follows. Step 1. Oil red A and B were mixed. 2. The mixture was filtered. 3. Sections were stained with mixture for 5 min. 4. Sections were washed by ddH$_2$O. 5. Sections were stained with hematoxylin for 20 s. 5. Sections were washed and were covered by glasses. Five randomly selected ×200 fields per slide were photographed in a blinded manner.

Cell count kit 8 (CCK-8)

CCK-8 kit (Beyotime, C0038) is an indirect cell viability detection method that was used to raw gradient centration detection or cell viability detection supplement method. In this study, this kit was used to select suitable alcoholic centration. First, a suitable number of cells were seeded in 96 well-plate ($3x10^3$-$5x10^3$ per well). Then, gradient centration of ethanol or gradient centration of metformin was added to cell plates. After 6 hours of incubation, 10 ul CCK-8 solution was added to each well. After another incubate time (2 h), the cell viability could be read at 450 nm by a microplate reader. CCK-8 results are representative of experiments from 4 separate plates.

Histopathology, immunohistochemical (IHC), and analysis method

A relative measuring method was used to estimate the liver vacuoles and the protein levels in the liver. Staining intensity (vacuole area) and stained cell ratio (vacuole ratio) were used to estimate the scores in every image. Stained cell percent: 1%–20% was marked 1 point, 21%–40% was marked 2 points, 41%–60% was marked 3 points, 61%–80% was scored 4 points, and 81%–100% was marked 5 points. Staining intensity: shallow yellow (small vacuole) was marked as 1 point, claybank (middle vacuole) was marked as 2 points, sepia

(huge vacuole) was marked as 3 points. Then, the protein level (liver impaired situation) was estimated by multiplying the results of the two separate points.

Serum level of GPT, GOT1, BUN activity assay

GPT, GOT1 and BUN levels in serum from C57BL/6 J mice were assayed using GPT, GOT1, BUN activity assay kits (Nanjing Jiancheng Bioengineering, C009-2-1, C010-2-1, C013-2-1). The absorbance was measured at 510 nm (GPT, GOT1), and 640 nm (BUN) with a multi-function microplate reader.

Immunofluorescence (IF)

Liver sections were fixed by 4% paraformaldehyde (Sigma-Aldrich, P6148) at room temperature for 10 min, and sections were washed with PBS 3 times, permeabilized, and blocked in 3% BSA in PBS containing 0.2% Triton X-100 (Sigma-Aldrich, X100) for 1 h. Primary antibodies (LC3 [bios, bs-8878 r], TOMM20 Santa Cruz Biotechnology, sc-166,729]) were diluted in 3% BSA (Sigma-Aldrich, A2153) for overnight incubation. Sections were washed with PBS and subsequently incubated with Alexa Fluor 488 (ZSGB-bio, ZF-051) or rho-damine-conjugated (ZSGB-bio, ZF-0313) secondary antibodies. The nucleus was labeled with Hoechst 33,342 (Thermo Fisher Scientific, H3570) at room temperature for 10 min. An Olympus fluorescence microscope was used to image the cells. Merged signal (yellow point) were counted in five randomly chosen microscopy fields. All experiments were repeated three times.

Western blot (whole-cell lysis and mitochondrial lysates)

Whole-cell lysates: liver tissue (200 mg) was mechanically homogenized with 1 ml of RIPA buffer, contained 1% protease inhibitor complex (Sigma-Aldrich, P2714), and the tissue homogenates were kept on ice for 30 min to total cell lysis. Mitochondrial protein: cells and tissues were treated by pre-chilled mitochondrial extraction buffer (220 mM D-Mannitol [Sigma-Aldrich, M4125], 70 mM sucrose [Sigma-Aldrich, V900116], 20 mM HEPES-KOH [Sigma-Aldrich, P5958], pH 7.5, 1 mM EDTA, 0.5 mM phenyl-methylsulfonyl fluoride [Sigma-Aldrich, P7626]. 2 mg/ml BSA [Sigma-Aldrich, A2153], supplemented with protease inhibitors including 10 μg/ml aprotinin [Sigma-Aldrich, Y0001154], 1 μM pepstatin A [Sigma-Aldrich, EI10], and 10 μM leupeptin [Sigma-Aldrich, L2884]). Cells and tissue fragments were passed through the 25-G syringe 20 times on ice. The homogenized cells were centrifuged at $1,000 \times g$ for 15 min at 4°C. The supernatant was further centrifuged at $10,000 \times g$ for another 10 min at 4°C to pellet the mitochondria. The supernatant fraction was retained as the cytosolic fraction. The mitochondrial pellets were resuspended in RIPA buffer and then subjected to SDS-PAGE and immunoblotting. An equal amount of protein (40–50 μg) was loaded on 10% SDS-PAGE wells and was transferred onto PVDF (Sigma-Aldrich, IPVH00010) membranes. The membranes were blocked by TBST (Tris-buffered saline [Sigma-

Aldrich, T6664] with 0.05% Tween 20 [Solarbio, T8220]) containing 5% nonfat milk for 2 h. Membranes were washed three times (5 min per time) by TBST and were probed with 1:200–1:1000 diluted antibodies of anti-AMPK (Abcam, ab32047), anti-p-AMPK (Abcam, ab133448), anti-PRKN /Parkin (Abcam, ab77924, UK), anti-PINK1 (Abcam, ab23707), anti-mitochondrial complex (Abcam, ab110413), anti-UQCRC2 (Santa Cruz Biotechnology, sc-39,037, US), anti-TOMM20 (Santa Cruz Biotechnology, sc-166,729), anti-LC3 (bios, bs-8878 r), anti-NFE2L2/NRF2 (Abcam, ab137550)antibodies to monitor proteins. After three steps of wash, membranes were incubated in secondary anti-rabbit or anti-mouse antibody conjunct HRP agent (1:7500 dilution; ZSGB-bio, ZDR-5306; ZSGB-bio, ZDR-5307) for 2 h at room temperature. After three times washed by TBST, membranes were visualized with ECL-chemiluminescent kit (ECL-plus; Thermo Scientific, 34,095). Then band images could be shot by the camera and stored by the computer. Then membranes were re-incubated with ACTB (loading control for whole cell lysates; bios, bsm-33,036 m) and TOMM20 (loading control for mitochondrial lysates). The next day, the control loading images could be shot. ImageJ densitometry software (Version 1.41) was used to transfer the image to data. And all data were calculated by at least three images.

Mitochondrial respiratory chain activity

Mitochondrial respiratory activity kits (Solarbio, BC0510, BC32330, BC3245, BC1445) were chosen to detect mitochondrial activity (I, II, III, and V). The mitochondrial complex was obtained by differential centrifugation. Mitochondrial lysates and reagents were added into microplates according to the procedure and were measured by a microplate reader.

Total RNA extraction and quantitative real-time PCR (qRT-PCR)

Total RNA in cells and tissues was extracted using TRIzol reagent (Invitrogen, 15,596,026), and the first-stand cDNA was synthesized using the First Strand cDNA Synthesis kit (TaKaRa, RR047A). qRT-PCR was performed with SYBR Green Master Mix (TaKaRa, R820A), and CFX-96 real-time PCR system (Bio-Rad, USA) was used to detect the mRNA fold changes in each sample. Sequences for qRT-PCR primers are shown below: *Actb/β-actin* (forward: 5′-CCCATCTATGAGGGTTACGC-3′; reverse: 3′-TTTAATGTCACGCACGATTTC-5′), *Uqcrc2* (forward: 5′-CAGACTCTGGGCTCTTTGGA-3′; reverse: 5′-TTGTTCTTGGCAGCTTGGAC-3′), and *Nfe2l2* (forward: 5′-TTCACTGAACACGAGTCCCA-3′; reverse: 5′-GGCCGTTCTGTTTGACACTT-3′), *Fasn* (forward: 5′-GGAGGTGGTGATAGCCGGTAT-3′; reverse: 3′-GGAGGTGGTGATAGCCGGTAT-5′), *Acaca*/ACC (forward:5′-GATGAACCATCTCCGTTGGC-3′ reverse:3′-GACCCAATTATGAATCGGGAGTG-5′), *Cpt1a* (forward:5′-ACAGTTGGCACAATAGACGTTT-3′ reverse:3′-CCTTCCATTTCAGTGTTGCAGA-5′) *Acadm*/MCAD

(forward:5′-ATGACGGAGCAGC CAATGAT-3′, reverse: 3′-TCGTCACCCTTCTTCTCTGCTT-5′).

The *MT-CO3* (mitochondrially encoded cytochrome c oxidase III) primer (forward: 5′- ACCAAGGCCACCACACTCCT-3′; reverse: 5′-ACGCTCAGAAGAATCCTGCA AAGAA- 3′) were used to detect the relative expression of mtDNA.

RNA-seq

Total RNA was extracted by TRIzol, and NanopDrop 2000 spectrophotometer (ThermoFisher) was used to determine RNA concentration. mRNA was enriched with magnetic beads containing oligo(dT), and Fragmentation Buffer was added to the mRNA to cut fragments into short fragments. Then, short fragments were used as templates to synthesize the first cDNA strand with random hexamers. Buffer, dNTPs, RNase H, and DNA polymerase I were added to synthesize the second cDNA strand. After purification (QiaQuick PCR kit, 28,104), cDNAs were repaired and were added with base A. Then were recovered with the target size fragments by agarose gel electrophoresis. PCR amplification was conducted to complete the entire library preparation. HiSeq2000 (Illumina) was used for the sequencing of the constructed library.

Electron microscopy

Mice livers were fixed with a combination of paraformaldehyde and glutaraldehyde, and the cells and livers were processed and sectioned with a diamond knife on copper grids after fixation. Grids were examined with a Hitachi (Tokyo, Japan) 7100 electron microscope, and images were captured using a MegaView III digital camera (Soft Imaging System, USA). Quantification of TEM was counted in five randomly chosen microscopy fields. All experiments were repeated three times.

Chromatin immunoprecipitation assays (ChIP)

Chromatin immunoprecipitation assays were performed using a ChIP assay kit (Beyotime, P2078), according to manufacturer instructions. For cells, AML-12 cells were treated with 3.2 mM metformin or vehicle for 24 h. Proteins bound to DNA were cross-linked by adding formaldehyde to a final concentration of 1% for 30 min at 37°C and the cross-linking was stopped by the addition of glycine to a final concentration of 0.125 M. Cells were then washed twice in ice-cold PBS containing protease inhibitors, pelleted, resuspended in 200 μl SDS lysis buffer (Beyotime, P2078-11), and sonicated in an ultrasonic processor (Bioruptor Plus, Belgium) to an approximate DNA size of 500 bp. Samples were pre-cleared with protein G agarose beads (Beyotime, P2078-1). Samples were then immunoprecipitated with anti-NFE2L2 antibody (Abcam, ab137550) or IgG (Millipore, 12–370) overnight at 4°C. Chromatin protein/DNA complexes were eluted from the agarose beads twice by adding 100 μl of elution buffer (1% SDS and 0.1 M NaHCO$_3$, pH 8.0) at room temperature for 15 min. Cross-linking was reversed by heating to 65°C for 4 h. DNA fragments were purified and were amplified by real-time PCR using SYBR green (TAKARA, R820A), with the *Uqcrc2* primers.

Luciferase reporter assays

The AML-12 cells were cultured in 96-well plates 24 h before transfection and then cotransfected with 100 ng pGL3-*Nfe2l2* and pcDNA3.1-*Uqcrc2* promoter-luciferase reporter plasmid or the negative controls by using Lipofectamine 2000 reagent (11,668,019, Invitrogen) according to the manufacturer's instructions. The Firefly and Renilla luciferase activities were measured using the Dual-Luciferase Reporter Assay System (Promega, E1960) 48 h after transfection, as described by the manufacturer. Renilla luciferase activity was normalized to Firefly luciferase activity. Construction of reporter plasmids and luciferase assay were performed by Hanbio (Shanghai, China).

Statistical analysis:

All data were analyzed by PRISM 7.0 version software. And all results were presented as means ± SD. In all graphs, Statistical significance was analyzed by Student's t-test.

Disclosure statement

The authors declare no conflict of interest.

ORCID

Xinyi Lu http://orcid.org/0000-0002-9634-2333

References

[1] Sarin SK, Kumar M, Eslam M, et al. Liver diseases in the Asia-Pacific region: a lancet gastroenterology & hepatology commission. Lancet Gastroenterol. 2020;5(2):167–228

[2] Gao B, Bataller R. Alcoholic liver disease: pathogenesis and new therapeutic targets. Gastroenterology. 2011;141(5):1572–1585

[3] Lu X, Liu YR, Xuan WT, et al. Circ_1639 induces cells inflammation responses by sponging miR-122 and regulating TNFRSF13C expression in alcoholic liver disease. Toxicol Lett. 2019;314:89–97

[4] Klionsky DJ, Abdelmohsen K, Abe A, et al. Guidelines for the use and interpretation of assays for monitoring autophagy (3rd edition). Autophagy. 2016;12(1):1–222

[5] Lemasters JJ, Zhong Z. Mitophagy in hepatocytes: types, initiators and role in adaptive ethanol metabolism. Liver Res. 2018;2 (3):125–132

[6] Williams J, Ding WX. Mechanisms, pathophysiological roles, and methods for analyzing mitophagy – recent insights. Biol Chem. 2017;1437–4315

[7] Xian H, Liou YC. Loss of MIEF1/MiD51 confers susceptibility to BAX-mediated cell death and PINK1-PRKN-dependent mitophagy. Autophagy. 2019;15(12):2107–2125

[8] Ahmad T, Sundar IK, Lerner CA, et al. Impaired mitophagy leads to cigarette smoke stress-induced cellular senescence: implications for chronic obstructive pulmonary disease. Faseb J. 2015;29(7):1–18

[9] Garcia D, Shaw RJ. AMPK: mechanisms of cellular energy sensing and restoration of metabolic balance. Mol Cell. 2017;66(6):789–800

[10] Cittadini A, Napoli R, Monti MG, et al. Metformin prevents the development of chronic heart failure in the SHHF rat model. Diabetes 2012;61(4):944–953

[11] Li Y, Xu S, Mihaylova MM, et al. AMPK phosphorylates and inhibits SREBP activity to attenuate hepatic steatosis and atherosclerosis in diet-induced insulin-resistant mice. Cell Metab. 2011;13(4):376–388

[12] Pei S, Minhajuddin M, Adane B, et al. AMPK/FIS1-mediated mitophagy is required for self-renewal of human aml stem cells. Cell Stem Cell. 2018;23(1):86–100

[13] Chen JL, Luo C, Pu D, et al. Metformin attenuates diabetes-induced tau hyperphosphorylation in vitro and in vivo by enhancing autophagic clearance . Experimental Neurology. 2019;311:44–56

[14] Lin S-C, Hardie DG. AMPK: sensing Glucose as well as Cellular Energy Status. Cell Metab. 2018;27(2):299–313

[15] Herzig S, Shaw RJ. AMPK: guardian of metabolism and mitochondrial homeostasis. Nat Rev Mol Cell Biol. 2018;19(2):121–135

[16] Kusminski CM, Scherer PE. Mitochondrial dysfunction in white adipose tissue. Trends Endocrinol Metab. 2012;23(9):435–443

[17] Laker RC, JC Drake, RJ Wilson, et al. Ampk phosphorylation of Ulk1 is required for targeting of mitochondria to lysosomes in exercise-induced mitophagy. Nat Commun. 2017;8(1):1–13

[18] Weinberg SE, Sena LA, Chandel NS. Mitochondria in the regulation of innate and adaptive immunity. Immunity. 2015;42(3):406–417

[19] Ma X, Xu L, Alberobello T, et al. Celastrol protects against obesity and metabolic dysfunction through activation of a HSF1-PGC1alpha transcriptional axis. Cell Metab. 2015;22(4):695–708

[20] Williams JA, Ni HM, Ding Y, et al. Parkin regulates mitophagy and mitochondrial function to protect against alcohol-induced liver injury and steatosis in mice. Am J Physiol Gastr L. 2015;309(5):324–340

[21] Mauro-Lizcano M, Esteban-Martinez L, Seco E, et al. New method to assess mitophagy flux by flow cytometry. Autophagy. 2015;11 (5):833–843

[22] Li Y, Xue Y, Xu X, et al. A mitochondrial FUNDC1/HSC70 interaction organizes the proteostatic stress response at the risk of cell morbidity. Embo J. 2019;38(3):1–20

[23] Steinberg GR, Kemp BE. AMPK in health and disease. Physiol Rev. 2009;89(3):1025–1078

[24] Fullerton MD, Galic S, Marcinko K, et al. Single phosphorylation sites in Acc1 and Acc2 regulate lipid homeostasis and the insulin-sensitizing effects of metformin. Nat Med. 2013;19(12):1649–1654

[25] You Y, Li WZ, Zhang S, et al. SNX10 mediates alcohol-induced liver injury and steatosis by regulating the activation of chaperone-mediated autophagy. J Hepatol. 2018;69(1):129–141

[26] Rabinovitch RC, Samborska B, Faubert B, et al. AMPK maintains cellular metabolic homeostasis through regulation of mitochondrial reactive oxygen species. Cell Rep. 2017;21(1):1–9

[27] Dudek J. Role of cardiolipin in mitochondrial signaling pathways. Front Cell Dev Biol. 2017;5:1–17.

[28] Chu CT, Ji J, Dagda RK, et al. Cardiolipin externalization to the outer mitochondrial membrane acts as an elimination signal for mitophagy in neuronal cells. Nat Cell Biol. 2013;15(10):1197–1205

[29] Ray NB, Durairaj L, Chen BB, et al. Dynamic regulation of cardiolipin by the lipid pump Atp8b1 determines the severity of lung injury in experimental pneumonia. Nat Med. 2010;16 (10):1120–1127

[30] Maekawa S, Takada S, Nambu H, et al. Linoleic acid improves assembly of the CII subunit and CIII2/CIV complex of the mitochondrial oxidative phosphorylation system of the heart failure. Cell Commun Signal. 2019;17(128):1–11

[31] Chomova M, Balazova M, Muchova J. Diabetes-induced abnormalities of mitochondrial function in rat brain cortex: the

effect of n-3 fatty acid diet. Mol Cell Biochem. 2017;435(1–2):109–131

[32] Wang Y, Hekimi S. Understanding Ubiquinone. Trends Cell Biol. 2016;26(5):367–378

[33] Mourier A, Motori E, Brandt T, et al. Mitofusin 2 is required to maintain mitochondrial coenzyme Q levels. J Cell Biol. 2015;208 (4):429–442

[34] Shin H, Kim H, Oh S, et al. AMPK–SKP2–CARM1 signalling cascade in transcriptional regulation of autophagy. Nature. 2016;534(7608):553–557

[35] Akimov V, Barrio-Hernandez I, Hansen S, et al. UbiSite approach for comprehensive mapping of lysine and N-terminal ubiquitination sites. Nat Struct Mol Biol. 2018;25(7):631–640

[36] Udeshi ND, Svinkina T, Mertins P, et al. Refined preparation and use of Anti-K-ε-GG antibody enables routine quantification of 10,000's of ubiquitination sites in single proteomics experiments. Mol Cell Proteomics. 2013;12(3):825–831

[37] Luessen DJ, Sun H, McGinnis MM, et al. Acute ethanol exposure reduces serotonin receptor 1A internalization by increasing ubiquitination and degradation of beta-arrestin2. J Biol Chem. 2019;294(38):14068–14080

[38] Cui W, et al. Nrf2 attenuates inflammatory response in COPD/emphysema: crosstalk with Wnt3a/β-catenin and AMPK pathways. J Cell Mol Med. 2018;22(7):3514–3525.

[39] Xu D, Xu M, Jeong S, et al. The role of Nrf2 in liver disease: Novel molecular mechanisms and therapeutic approaches. Front Pharmacol. 2018;9:1–7

[40] Wang Z, Chen Z, Jiang P, et al. Cordycepin prevents radiation ulcer by inhibiting cell senescence via NRF2 and AMPK in rodents. Nat Commun. 2019;10(1):2538

[41] Lv H, Liu Q, Wen Z, et al. Xanthohumol ameliorates lipopolysaccharide (LPS)-induced acute lung injury via induction of AMPK/GSK3beta-Nrf2 signal axis. Redox Biol. 2017;12:311–324

[42] Cuadrado A, Kugler S, Lastres-Becker I. Pharmacological targeting of GSK-3 and NRF2 provides neuroprotection in a preclinical model of tauopathy. Redox Biol. 2018;14: 522–534

[43] Huang XT, Liu W, Zhou Y, et al. Galectin-1 ameliorates lipopolysaccharide-induced acute lung injury via AMPK-Nrf2 pathway in mice. Free Radic Biol Med. 2020;146:222–233

[44] Cederbaum AI. Alcohol metabolism. Clin Liver Dis. 2012;16 (4):667–685.

[45] Demine S, Renard P, Arnould T. Mitochondrial uncoupling: a key controller of biological processes in physiology and diseases. Cells. 2019;8(8):1–40

[46] Kenwood BM, Weaver JL, Bajwa A, et al. Identification of a novel mitochondrial uncoupler that does not depolarize the plasma membrane. Mol Metab. 2014;3(2):114–123

[47] Han Y, Hu Z, Cui A, et al. Post-translational regulation of lipogenesis via AMPK-dependent phosphorylation of insulin-induced gene. Nat Commun. 2019;10(1):1–13

[48] Ni HM, Chao X, Yang H, et al. Dual roles of mammalian target of rapamycin in regulating liver injury and tumorigenesis in autophagy-defective mouse liver. Hepatology. 2019;70(6):2142–2155

[49] Lazarou M, Sliter DA, Kane LA, et al. The ubiquitin kinase PINK1 recruits autophagy receptors to induce mitophagy. Nature. 2015;524(7565):309–314

[50] Gelmetti V, Rosa PD, Torosantucci L, et al. PINK1 and BECN1 relocalize at mitochondria-associated membranes during mitophagy and promote ER-mitochondria tethering and autophagosome formation. Autophagy. 2017;13(4):654–669

[51] Okatsu K, Oka T, Lguchi M, et al. PINK1 autophosphorylation upon membrane potential dissipation is essential for Parkin recruitment to damaged mitochondria. Nat Commun. 2012;3(1):1–10

[52] Safiulina D, Kuum M, Choubey V, et al. Miro proteins prime mitochondria for Parkin translocation and mitophagy. Embo J. 2018;38(2):1–18

[53] Hasson SA, Kane LA, Yamano K, et al. High-content genome-wide RNAi screens identify regulators of parkin upstream of mitophagy. Nature. 2013;504(7479):291–295

[54] Seo E, Park EJ, Joe Y, et al. Overexpression of AMPKalpha1 ameliorates fatty liver in hyperlipidemic diabetic rats. Korean J Physiol Pharmacol. 2009;13(6):449–454

[55] Zhang HA, Yang XY, Xiao YF. AMPKalpha1 overexpression alleviates the hepatocyte model of nonalcoholic fatty liver disease via inactivating p38MAPK pathway. Biochem Biophys Res Commun. 2016;474(2):364–370

[56] Mottillo EP, Desjardins EM, Crane JD, et al. Lack of adipocyte ampk exacerbates insulin resistance and hepatic steatosis through brown and beige adipose tissue function. Cell Metab. 2016;24(1):118–129

[57] Smith BK, Marcinko K, Desjardins EM, et al. Treatment of non-alcoholic fatty liver disease: role of AMPK. Am J Physiol Endocrinol Metab. 2016;311(4):730–740

[58] Bertola A, Mathews S, Ki H, et al. Mouse model of chronic and binge ethanol feeding (the NIAAA model). Nat Protoc. 2013;8 (3):627–637